Impacts of glacial runoff on phytoplankton biomass, activity and composition in South-West Greenland fjord system

Master Thesis

Vilma Ihalainen

The Department of Environmental Science

Aquatic Sciences

Helsinki University

October 2020

HELSINGIN YLIOPISTO
HELSINGFORS UNIVERSITET
UNIVERSITY OF HELSINKI

Tiedekunta – Fakultet – Faculty Bio- ja ympäristötieteellinen tiedekunta	Koulutusohjelma – Utbildningsprogram – Degree Programme Akvaattisten tieteiden koulutusohjelma	
Tekijä – Författare – Author Vilma Ida Adina Ihalainen		
Työn nimi – Arbetets titel – Title Jäätikön sulamisen vaikutukset vuonon perustuotantoon sekä kasviplanktonin koostumukseen ja biomassaan Lounais-Grönlannissa		
Oppiaine/Opintosuunta – Läroämne/Studieinriktning – Subject/Study track Meribiologia		
Työn laji – Arbetets art – Level Pro Gradu -tutkielma	Aika – Datum – Month and year 10 / 2020	Sivumäärä – Sidoantal – Number of pages 54s + liitteet 7s

Tiivistelmä – Referat – Abstract

Nykyisellä ilmaston lämpenemisellä on ennennäkemättömiä vaikutuksia Grönlannin vuonoihin ja niihin yhteydessä olevien jäätiköiden sulamiseen. Vedenpinnan alapuolisen jään sulaessa makean sulamisveden virtaus meren pintakerrokseen kasvaa, mikä johtaa lisääntyneeseen ravinteiden kumpuamiseen. Tässä tutkimuksessa tarkastellaan ympäristötekijöitä, jotka vaikuttavat arktisen vuonon perustuotantoon, kasviplanktonin runsauteen ja biomassaan (klorofylli *a*) sekä kasviplanktonyhteisöjen lajikoostumukseen. Tutkimus toteutettiin Lounais-Grönlannissa Godthåbsfjord -vuonolla vuoden 2019 elokuussa. Näytteet kerättiin vuonoa pitkin jäätikön reunalta vuonon suulle.

Kumpuaminen jäätiköiden edustalla sekä rannikkoveden virtaus vuonoon olivat yhteydessä typpi- ja fosfaattipitoisuuksien vaihteluihin, kun taas silikaattipitoisuuksien jakautuminen ei noudattanut vesimassojen liikkeitä. Kasviplanktonin biomassan jakaantuminen selittyi typpipitoisuuksien vaihtelulla yhdessä fosfaatti- ja suolapitoisuuksien sekä syvyyden kanssa. *Chaetoceros socialis* -piilevä oli ylivoimaisesti runsain kasviplanktonlaji (≥ 90%) silikaattirajoitteisissa vesissä ja lajin esiintyvyys vaikutti koko kasviplanktonyhteisön ympäristövasteisiin. *C. socialis* -lajin suuri suhteellinen runsaus oli myös yhteydessä korkeaan lajirunsauteen. Miksotrofisen *Dinobryon balticum* -kultalevän runsas esiintyvyys (9–46%) oli usein yhteydessä matalaan typpipitoisuuteen.

Lajirunsaus ja *C. socialis* -lajin osuus kasvoivat lähempänä vuonon pohjukkaa. Myös kasviplanktonin runsaus ja biomassa (klorofylli a) olivat suuremmat lähempänä jäätiköitä, kun taas perustuotanto oli korkeampi lähempänä vuonon suuta. Tämä viittaa siihen, että sisempänä vuonoa syyskukinnan huippu oli tutkimushetkellä saavutettu, kun taas ulompana syyskukinta oli edelleen kehittymässä. Näin ollen jäätiköiden pinnanalainen sulaminen sekä sulamisvesien pintavalunta kasvattivat kasviplanktonin runsautta ja klorofylli *a* -pitoisuuksia, kun taas perustuotanto oli riippuvainen myös muista tekijöistä, kuten valon saatavuudesta ja veden pystysuuntaisesta sekoittumisesta.

Grönlannin jääpeitteen sulamisen ennustetaan kiihtyvän. Tämän takia myös ravinteiden kumpuaminen saattaa tulevaisuudessa kiihtyä, mikä luultavasti johtaa perustuotannon kasvuun. Lisääntyvä sulamisvesien pintavalunta saattaa myös nostaa silikaattipitoisuuksia, mikä hyödyttää piileviä. Toisaalta sulamisjokien ja valumaveden sameus rajoittaa perustuottajien valon saantia ja näin ollen lisääntynyt pintasulaminen voi myös johtaa perustuotannon heikentymiseen. Mikäli meriin suoraan yhteydessä olevat jäätiköt vetäytyvät mantereille, ravinteiden kumpuaminen hiipuu ja nopea typenkulutus pintakerroksesta johtaa perustuotannon laskuun. Ilmaston lämpeneminen ja jäätiköiden sulaminen muuttavat arktisten vuonojen tuottavuutta ja väistämättä muokkaavat alueiden rikkaita ja ainutlaatuisia ekosysteemejä.

Avainsanat – Nyckelord – Keywords
Arktinen kasviplankton, perustuotanto, jäätiköiden sulaminen, kumpuaminen, Godthåbsfjord, *Chaetoceros socialis*

Ohjaaja tai ohjaajat – Handledare – Supervisor or supervisors
Rolf Gradinger, Thomas Juul-Pedersen & Aleksandra Lewandowska

Säilytyspaikka – Förvaringställe – Where deposited

Muita tietoja – Övriga uppgifter – Additional information

HELSINGIN YLIOPISTO
HELSINGFORS UNIVERSITET
UNIVERSITY OF HELSINKI

Tiedekunta – Fakultet – Faculty Faculty of Biological and Environmental Sciences		Koulutusohjelma – Utbildningsprogram – Degree Programme Degree Programme in Aquatic Sciences
Tekijä – Författare – Author Vilma Ida Adina Ihalainen		
Työn nimi – Arbetets titel – Title Impacts of glacial runoff on phytoplankton biomass, activity and composition in South-West Greenland fjord system		
Oppiaine/Opintosuunta – Läroämne/Studieinriktning – Subject/Study track Marine Biology		
Työn laji – Arbetets art – Level Master Thesis	Aika – Datum – Month and year 10 / 2020	Sivumäärä – Sidoantal – Number of pages 54pp + 7pp appendices

Tiivistelmä – Referat – Abstract

Ongoing climate warming has unprecedented impacts on glacial melt and associated fjord systems in Greenland. As the glaciers are shrinking, freshwater inflow to the sea is increasing resulting in increased nutrient supply by upwelling. In this study I examined environmental factors impacting marine primary productivity, biomass (chlorophyll *a*), phytoplankton abundance and species composition along a transect from the glacier front to the outer fjord in Godthåbsfjord, SW-Greenland, in August 2019.

Gradients in nitrogen and phosphate concentrations were explained by glacial runoff and coastal water inflow while silicate concentration did not follow these patterns. The main variables explaining phytoplankton biomass distribution were nitrogen together with phosphate concentrations, salinity, and depth. Silicate limited waters were strongly dominated (≥ 90%) by the diatom *Chaetoceros socialis*, which had a strong influence on phytoplankton community response to environmental conditions. High dominance of *C. socialis* was also related to high species richness. Nitrogen depleted waters were usually related to relatively high abundances (9–46%) of mixotrophic *Dinobryon balticum*.

Higher number of species and higher dominance of *C. socialis* was detected closer to the glacier. Phytoplankton abundance and biomass (chlorophyll *a*) were higher in the inner fjord region, whereas primary productivity had the opposite pattern (higher productivity in the outer fjord). This suggested that an autumn bloom was peaking in the inner fjord, whereas in the outer fjord the autumn bloom was still developing. Thus, glacial surface runoff and subglacial discharge contributed to higher phytoplankton abundance and chlorophyll *a* concentrations, whereas primary production was also dependent on other factors such as light availability and vertical mixing.

Melting of Greenland Ice sheet is predicted to accelerate in the future. Thus, the upwelling effect might increase, leading to transitory increase in marine primary production. Increased surface runoff might increase silicate concentrations benefiting diatom species, although turbid runoff water will also decrease the primary productivity due to light limitation. Nevertheless, if marine-terminating glaciers retreat further and become land-terminating glaciers, lack of nutrient upwelling will lead to faster exhaustion of nitrogen in the upper water column and primary productivity will eventually decrease. Thus, global warming and retrieving of glaciers will change the productivity of the fjord and inevitably shape the rich and unique fjord ecosystems of the Arctic.

Avainsanat – Nyckelord – Keywords
Arctic phytoplankton, primary production, glacial melting, nutrient upwelling, Godthåbsfjord, *Chaetoceros socialis*

Ohjaaja tai ohjaajat – Handledare – Supervisor or supervisors
Rolf Gradinger, Thomas Juul-Pedersen & Aleksandra Lewandowska

Säilytyspaikka – Förvaringställe – Where deposited

Muita tietoja – Övriga uppgifter – Additional information

Abbreviations

Chl *a*	Chlorophyll *a*
CTD	Conductivity Temperature Depth probe
ENS	Effective Number of Species
IF	Inner Fjord
NOx	Dissolved Inorganic Nitrite (NO_2^-) and Nitrate (NO_3^-) combined
OF	Outer Fjord
P-I	Photosynthesis-Irradiance

Table of Contents

1. Introduction

Polar fjords are traditionally seen as an interface and buffer zone between glaciated continental shelves and the oceans offering a complex environment to arctic nature (Syvitski et al., 1987). Most glaciers of Greenland fjord systems are in a direct connection with the Greenland Ice Sheet. These fjord systems are characterized by glacier runoff, and additionally, river run off and tides are shaping the unique fjord environment both spatially and temporally.

The melting of the Greenland Ice sheet in Godthåbsfjord region has doubled over the last two decades (Van As et al., 2014). The key driving factor of this melting and fast glacier retreat is thought to be submarine tidewater glacial calving fronts (Slater et al., 2019; Straneo & Heimbach, 2013). The retreat of the glacial ice has been predicted to be strongest especially in South-West Greenland (Slater et al., 2019). As the glaciers are shrinking, freshwater inflow from glaciers is increasing not only by glacial meltwater rivers but also by increased calving of glacial fronts resulting increasing upwelling of nutrients (Bendtsen et al., 2015).

The Fjord-Glacier systems can be divided into those a) influenced directly by the glacial front (marine-terminating glaciers) and b) influenced by rivers coming from melting glaciers (land-terminating glaciers). One major difference is that marine-terminating glaciers introduce meltwater not only at the surface but also in the deeper layers causing nutrient upwelling. This nutrient upwelling occurs when the glacier front (or iceberg) is melting from below and this cold and fresh meltwater starts to rise based on density difference between saltwater, introducing nutrients from the deeper water layers back to surface water (Meire et al. 2017; Rysgaard et al., 2003). As glaciers are shrinking, glacier fronts are retreading towards mainland and change from marine-terminating glaciers to land-terminating glaciers with potential impacts on the hydrography and biology of the associated fjords.

Glacier fronts have strong impacts on a fjord's environment and ecology. When glacial ice meltwater is introduced at depth (i.e. sub-glacial discharge), e.g. in Godthåbsfjord (Juul-Pedersen et al., 2015; Meire et al., 2017; Mortensen et al., 2011, 2013) upwelling entrains deeper fjord waters rich in nutrients. Generally, inorganic nutrients and especially nitrate are considered controlling the phytoplankton based primary production in such high-latitude fjord system (Tremblay & Gagnon, 2009). Therefore, upwelling based nutrient additions increase productivity and support a rich fjord biota from microscopic phytoplankton to marine mammals. In contrast in fjords with land-terminating glaciers, meltwater enters the fjords at the surface,

lacking the upwelling effect induced by sub-glacial discharge and causing less rich biota (Meire et al., 2017). It has been predicted that in the future the melting glaciers are retreating towards and onto land and the transition from marine-terminating to land-terminating glaciers may cause a shift in the adjacent fjord's ecosystems (Meire et al., 2017). Therefore, it is critical to collect current information on marine-terminating glacial fjord systems to study the impact of glacial retreat over time.

Even though the tidewater glacial fjord Godthåbsfjord is a well-studied fjord system including ongoing monitoring efforts (Marine Basis-Nuuk monitoring programme, www.g-e-m.dk), only limited information about phytoplankton species composition and abundance has been available (Krawczyk et al., 2015, 2018; Arendt et al., 2010). Most of these studies are based on sampling with net hauls failing to capture small (< 20 µm) taxa and reporting only relative abundances (Arendt et al., 2010; Krawczyk et al., 2015). It is not surprising that a recent study (Krawczyk et al., 2018) showed phytoplankton counts from water samples offer different results than phytoplankton counts derived from net hauls.

Microplankton species succession in Godthåbsfjord and the influence by coastal inflows and run-off from the Greenland Ice Sheet was described by Krawczyk et al. (2015), presenting the seasonal succession of microplankton species based on monthly plankton net hauls between January 2006 and December 2010. According to this study the highest abundance of microplankton was contributed by diatoms, such as *Chaetoceros* spp. and *Thalassiosira* spp., followed by dinoflagellates, silicoflagellates, and heterotrophic ciliates. In this fjord system, two blooms were observed (Juul-Pedersen et al., 2015; Krawczyk et al., 2015). The spring bloom was dominated by diatoms including *Thalassiosira* spp. and *Fragilariopsis* spp. and the haptophyte species *Phaeocystis* sp.. *Thalassiosira* spp. were also found as dominating species in the inner fjord after the spring bloom (Arendt et al., 2010). The second summer-autumn phytoplankton bloom was again strongly dominated by diatoms, however by different species such as: *Chaetoceros decipiens*, *Chaetoceros curvisetus*, and *Chaetoceros wighamii* (Krawczyk et al., 2015). In another study (Krawczyk et al., 2018) *Chaetoceros* cf. *socialis* was found to be the most dominant species during autumn bloom and associated with fresher water conditions.

2. Research questions and hypotheses

The aim of this study was to determinate the effect of glacial freshwater input and associated physical and chemical variables on both the horizontal and vertical distribution of phytoplankton abundance, community composition, diversity and primary productivity.

Through a comparison of inner fjord (IF) with outer fjord (OF) properties I addressed the following two hypotheses based on the upwelling based nutrient addition: 1) Primary productivity, biomass (chlorophyll *a*) and phytoplankton abundance are higher in the IF than the OF stations (Arendt et al., 2010). Also, I hypothesized that closer to the glacier there is 2) a higher number of species and more evenly distributed community composition than in the OF stations (based on Shannon index figure in Krawczyk et al., 2018). For both hypotheses, the null hypothesis was that there was no significant difference between IF and OF stations.

3. Research area

Godthåbsfjord in South-West Greenland is situated next to Nuuk, the capital of Greenland. Godthåbsfjord is an approximately 190 km long fjord system with an average water depth of about 250 m and maximum depths > 600 m. The stations located in the IF are deeper than the stations located on top of shallower sills in the OF (Mortensen et al., 2011). Stations in the IF are strongly affected by glacial runoffs and tides (Mortensen et al., 2011).

Along the coast of South-West Greenland three water masses; Atlantic Water, Coastal Water, and Fresh water from glaciers with different physical features are introduced (Mortensen et al., 2011). Strong tidal mixing and narrow passageway formed by sill regions in the OF drive density gradients between IF and OF (Mortensen et al., 2011). Altogether there are six outlet glaciers in direct contact with the Greenland Ice sheet, three of them marine-terminating glaciers. These are Kangiata Nunâta Sermia at the end of the fjord, Akugdlerssûp Sermia 5km to south from Kangiata Nunâta Sermia and Narssap Sermia 50km outwards from the fjord-end (Figure 1; Mortensen et al., 2011). During summer, a persistent pycnocline is annually documented to form in the upper water layer, and this stratification effectively prevents mixing of coastal deeper water with the glacier meltwater (Juul-Pedersen et al., 2015; Krawczyk et al., 2015; Mortensen et al., 2011, 2013).

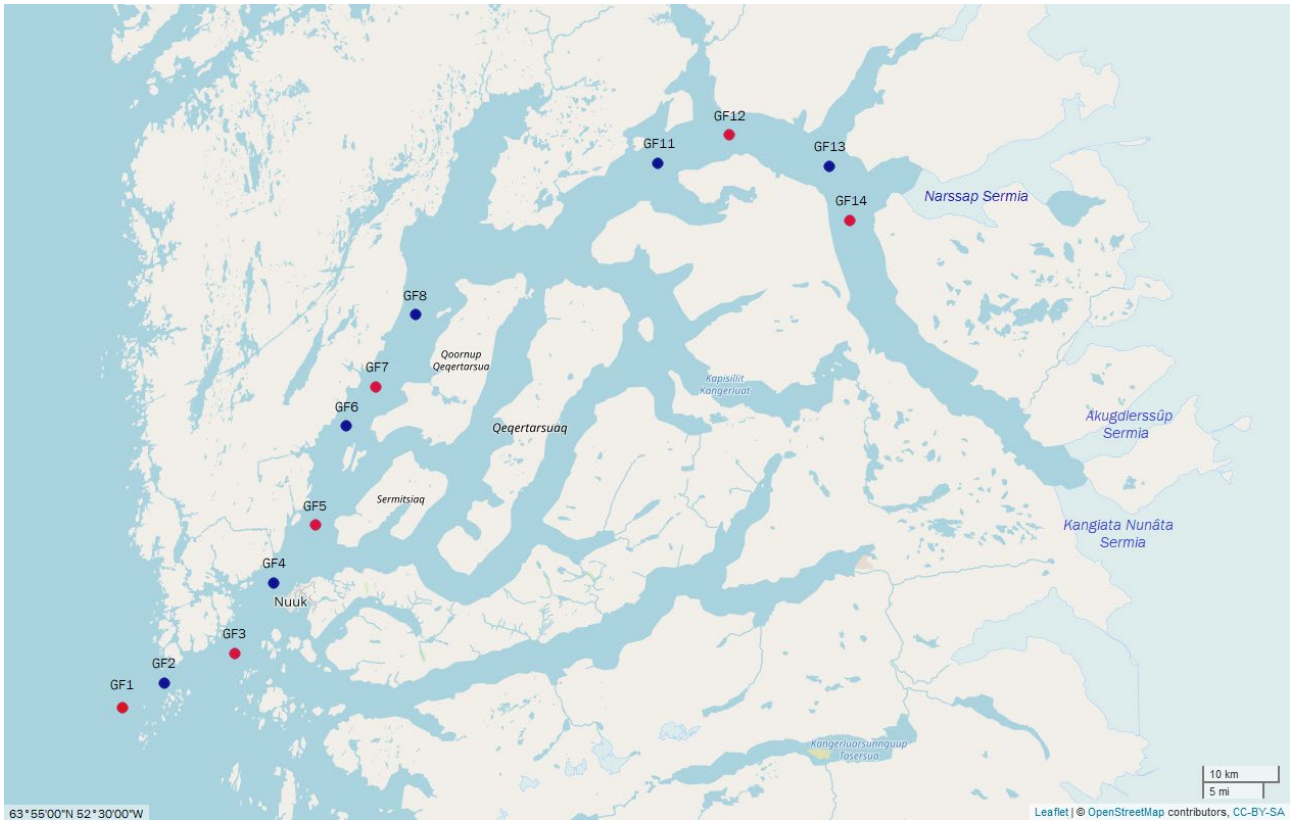

Figure 1 Map of the research area (OpenStreetMap 2019). Full stations are indicted by red dots and short stations by blue ones.

4. Methods

This study was conducted as a part of the Marine Basis-Nuuk monitoring programme, and the Greenland Ecosystem Monitoring (www.g-e-m.dk). Sampling was executed between 13.8.2019-17.9.2019 along a fjord transect. The fjord was divided into three sub-regions: the outermost stations (GF1, GF2 and GF3), the middle stations (GF4, GF5, GF6, GF7 and GF8) and the innermost stations (GF11, GF12, GF13 and GF14). There were two different station types: short stations (GF2, GF4 GF6, GF8, GF11 and GF13) and full stations (GF1, GF3, GF5, GF7, GF12 and GF14). Sampling at the short stations was limited to CTD (conductivity-temperature-depth) measurements for all the stations and chlorophyll *a* (chl *a*) analysis excluding stations GF11 and GF13. Sampling the full stations included previously mentioned variables and in addition nutrient analysis, primary productivity estimation and phytoplankton species composition and abundance. For the purpose of this study measurements within the upper 100 m of the water column were included. For the nutrient analysis water was obtained

from the depths of 5, 10, 20, 30, 40, 50 and 100 m. Phytoplankton was examined from the depths of 5 m, 20 m and 40 m and for the primary productivity experiment water was obtained from the depths of 5 m and 20 m. All water samples were taken with a 5-L Niskin bottle.

4.1 Physical environment

A SBE19plus CTD profiler equipped with a Seapoint Chlorophyll *a* Fluorometer and a Biospherical/Licor light sensor was used to measured pressure, temperature, salinity, irradiance (photosynthetically active radiation, PAR), and relative Chlorophyll a fluorescence. CTD measurements were taken at every station from the surface to approximately 20 m above the bottom with a 1 m resolution. Depth of the photic zone was defined as the depth where 1% of solar radiation penetrates the water column (Sverdrup, 1953). (In this research surface irradiance was defined from the depth of 1 m.) Sampling dates, locations, bottom depth and measurements of the stations are summarized in Table 1.

Table 1 Overview over sampling dates, station locations, water depths, performed analyzes and measurements. The last column includes visual assessment of the weather on the sampling day.

Station	Sampling day	Latitude N	Longitude W	Depth (m)	CTD	Chl a	Nutrients	Primary productivity	Phytoplankton	Weather
GF1	13.8.2019	64°03.053'	52°11.245'	320	x	x	x	x	x	Sunny, light breeze
GF2	13.8.2019	64°04.767'	52°04.525'	425	x	x				Sunny, light breeze
GF3	19.8.2019	64°06.866'	51°53.223'	370	x	x	x	x	x	Cloudy, calm
GF4	13.8.2019	64°11.483'	51°46.954'	405	x	x				Sunny, light breeze
GF5	13.8.2019	64°15.867'	51°40.069'	367	x	x	x	x	x	Sunny, light breeze
GF6	20.8.2019	64°22.788'	51°35.119'	640	x	x				Partly cloudy, moderate breeze
GF7	20.8.2019	64°25.514'	51°30.467'	636	x	x	x	x	x	Partly cloudy, moderate breeze
GF8	20.8.2019	64°30.552'	51°23.940'	639	x	x				Partly cloudy, moderate breeze
GF11	27.8.2019	64°41.052'	50°44.995'	568	x					Cloudy, calm
GF12	27.8.2019	64°43.022'	50°33.355'	542	x	x	x	x	x	Cloudy, calm
GF13	27.8.2019	64°40.800'	50°17.279'	492	x					Cloudy, calm
GF14	27.8.2019	64°37.070'	50°13.865'	460	x	x	x	x	x	Cloudy, calm

4.2 Nutrients

Nutrients were measured at the full stations at 5, 10, 20, 30, 40, 50, and 100 m water depth. Phosphate (PO_4^{3-}), silicate ($Si(OH)_4$) and nitrite (NO_2^-) plus nitrate (NO_3^-) were measured following the MarineBasis-Nuuk monitoring programme protocols (Juul-Pedersen et al., 2015;

Krawczyk et al., 2015). Water samples were filtered through a GF/C filter and kept frozen (-18 °C) prior to analysis. Phosphate and silicate concentrations were measured spectrophotometrically (Grasshoff et al., 1983; Strickland & Parsons, 1972). Nitrate and nitrite concentrations were measured following the vanadium chloride reduction method (García-Robledo et al., 2014). All nutrient analyzes were made with a Shimadzu UV-vis mini-1240 spectrophotometer.

4.3 Chlorophyll *a*

Chlorophyll *a* and phaeopigments were measured at each station at the depths of 5, 10, 20, 30, 40, 50 and 100 m following the MarineBasis-Nuuk monitoring programme protocols (Juul-Pedersen et al., 2015; Krawczyk et al., 2015). Briefly, 300 ml water samples were filtered through GF/C Whatman filters, extracted in 10 ml 96 % ethanol for 18 h and analyzed with a Turner Design Trilogy-1 fluorometer (Krawczyk et al., 2015). After initial reading three drops of 1M HCl acid were added and samples were measured again to distinguish between chlorophyll *a* and phaeopigment concentrations.

4.4 Phytoplankton

Phytoplankton samples were examined from the full stations from three depths: 5 m, 20 m, and 40 m. 250 ml water samples were preserved with 2 ml acidic Lugol's iodine solution and analyzed at UiT – The Arctic University of Norway in Tromsø using the Utermöhl method (Utermöhl, 1958). Samples were gently turned up and down for 10 minutes and then poured into 50 ml settling chambers and kept still 24 h before examination by inverted light microscope (Zeiss Primovert). Cells were identified and counted in a two-step approach counting a minimum of 500 cells or at least half of the sample. Small and abundant species were counted within sight of views with 40x objective whereas rare and bigger cells and colonies were counted on full chamber transacts with 10x object. When examining half or the whole chamber area for cells, the 20x objective was used. Counting methods followed HELCOM guidelines (HELCOM, 2017). Identification of species was based on Meunier (1910), Tomas (1997), Throndsen et al. (2007) and Karlson et al. (2018). Species diversity of the phytoplankton community was determined by species richness measured as the number of species, the effective number of species (ENS; Chase & Knight, 2013), the Shannon's diversity index (Shannon, 1948) and Pielou's evenness index (Pielou, 1966).

4.5 Primary productivity

Primary productivity was measured using water samples from 5 m and 20 m using the ^{14}C incorporation technique (Steeman Nielsen, 1952) and P-I (photosynthesis-irradiance) curves approach. Water from each depth was subsampled into 11 parallel light bottles and 3 control bottles. ^{14}C was added to each light bottle and control bottles. The control bottles were then placed into a lightproof metal box and the light bottles were placed side-by-side in a light incubator with running water (ca. 2.5˚C). A light diffusive end of the incubator allowed light from an external light source to enter the incubator. Light attenuation along the bottle series produced a decreasing light gradient. The light bottles were incubated for ca. 2 h, and experiments were terminated by removing the light bottles into a dark metal box. Immediately after ending the incubation, samples were filtered through GF/C filters. 100 µl 1 M HCl was added and filters were left to fumigate for 24 hours in a fume hood in order to remove remaining inorganic ^{14}C. 10 ml of Perkin Elmer scintillation Ultima Gold scintillation liquid was added to the samples before analyzes on a scintillation analyzer (Liquid Scintillation Analyzer, Tri-Carb 2800TR, PerkinElmer).

P-I curves were created using primary production values combined with light intensities measured inside each light bottle in the incubator. Daily incoming solar irradiance (PAR) was measured using a spherical light sensor (Li-COR Spherical PAR Sensor) located on the roof of the institute building during the sampling week. Primary productivity was calculated with interpolated P-I curves, daily incoming solar irradiance, *in situ* irradiance from CTD profiler and measured fluorescence (chlorophyll *a*) along with the calculated light attenuation for every depth from the surface down to 50 m depth. The primary productivity based on these datasets was calculated using the R statistical software (version 1.1.463; R Core Team, 2018) and R package *phytotool* (Silsbe & Malkin, 2015) with methods described by Platt and Sathyendranath (1995). Fitted P-I curves were calculated using the equation based on Webb et al. (1974):

$$y = alpha\ ek\ (1 - e^{-x/ek})$$

with *y* representing photosynthetic rate, *x* representing PAR data, and *alpha* and *ek* being parameter estimates.

4.6 Statistics

To quantitatively explore linear relationships between bathymetry (distance from the glacier and depth), physical and chemical predictors, a principal component analysis (PCA) was performed (Rao, 1964). PCA was based on the covariance matrix and variables were normalized prior the analysis to make sure that variances are on the same scale. Since the outermost glacier outlet Narssap Sermia is located in between GF13 and GF14 and the two innermost glaciers Kangiata Nunâta Sermia and Akugdlerssûp Sermia are located past GF14 in the end of the fjord, distance to the glaciers was calculated as a distance to GF14 through every station location in between.

Similarity of phytoplankton community composition between the stations was visualized with multidimensional scaling (MDS) plots based on Jaccard's and Bray-Curtis' similarity indices. Jaccard's similarity index is based on presence/absence data overestimating the impact of rare species (Jaccard, 1912), whereas Bray-Curtis similarity considers species relative abundances (Bray & Curtis, 1957). Also, hierarchical cluster analysis was done with both Jaccard and Bray-Curtis indices (Murtagh, 1985).

To test the linear effects of physical and chemical environment on phytoplankton biomass and diversity, I used linear regression models. PC1 and PC2 values were used as explanatory variables to account for collinearity between the predictors. Significant relationships ($p < 0.05$) indicate that the set of predictors, which explain each principal component, was driving the response. Chlorophyll *a* values were logarithmically transformed to fulfill the assumptions of normality and variance homogeneity of model residuals.

All statistical analyses were performed using R statistical software, including packages *factoextra* for PCA (Kassambara & Mundt, 2020) and *ggplot2* for graphics (Wickham, 2016). Diversity indices were calculated using R package *vegan* (Oksanen et al., 2019). Map of the research area was plotted using R package *leaflet* (Cheng et al., 2018) and transect contour plots were plotted using Ocean Data View (version 5.2.1; Schlitzer, 2020).

5. Results

5.1 Physical environment

5.1.1 Temperature

All stations showed a very intense vertical temperature gradient with highest temperatures close to the surface (Figure 2). At the middle stations surface temperature values were higher than in the outer or inner fjord (Table 2). Along the transect, the lowest surface temperature value was at GF14 (3.7˚C) whereas the highest temperature was in GF4 (9.7˚C; Table 2). From GF14 until GF8 temperature decreased from the surface values to 1˚C at the depth of 20 m and increased after that to 2˚C. The intermediate cold-water layer (i. e. cold water lens) was thickest close to the glacier and became narrower towards the OF. At GF7 and GF6 the thermocline was located at around 5 m and below it the water was 2˚C. At GF5 and GF4, relatively high surface temperatures dropped to 1˚C around 15 m depth and increased to 4˚C around 50 m. In the deeper waters the temperature dropped again to 2˚C.

At GF3, surface temperature was around 5˚C and 4˚C water extended down to 50 m depth. After that temperature decreased slowly to 3.2˚C at 100 m. In all the other stations temperatures below 60 m depth was below 3.0 ˚C and increased slightly from the IF outwards.

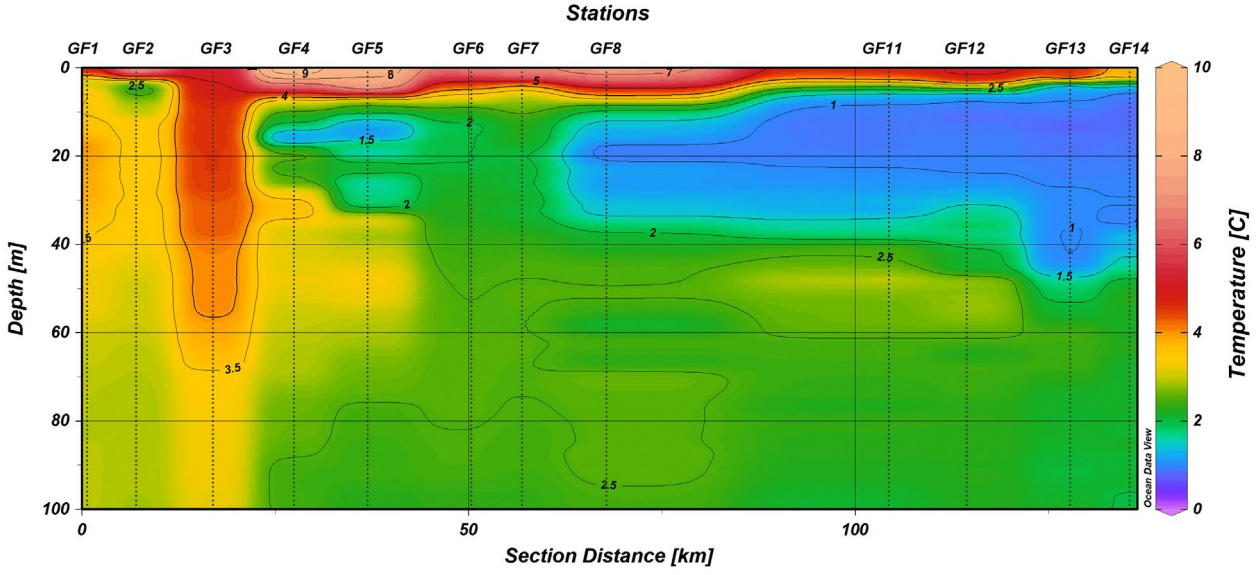

Figure 2 Temperature vertical distribution along the fjord transect in the upper 100 m of the water column. Datapoints are from every 1 m shown as vertical dotted lines.

Table 2 Surface temperature (˚C) and salinity at the depth of 1 m

Station	Temperature (˚C)	Salinity
GF1	4.8	27.7
GF2	7.5	21.2
GF3	5.2	28.1
GF4	9.7	17.9
GF5	8.4	18.0
GF6	6.6	18.1
GF7	7.1	15.9
GF8	7.5	15.6
GF11	4.7	5.4
GF12	5.3	5.9
GF13	4.6	5.7
GF14	3.8	6.9

5.1.2. Salinity

The salinity gradient (Figure 3) was following the temperature gradients (Figure 2). Salinity was highly stratified in the uppermost 5 m at the IF from GF14 to GF4 (i.e. fresh surface layer was discovered in the innermost and middle stations; Table 2). Contrary to the temperature, salinity increased steadily from the surface water until 100 m depth. Within the sub-regions salinity gradients did not vary whereas between the groups salinity was different. At the outermost stations more saline water (S ≥ 30.0) was found closer to the surface. At the middle stations less saline water (S < 30.0) extended from the surface down to 30-40 m depth. The deep salinity gradient was similar in IF and OF, but surface values were much lower at the innermost stations. At the outermost stations both deep water and surface salinity was higher than at the innermost and middle stations. The vertical mixing of the water at GF3 was evident from the salinity and temperature data. Here warm water (4˚C) having relatively low salinity (S ≥ 32) water extended to 50 m water depth. At the inner stations the 31.5 salinity gradient was linked to bottom of a cold-water lens (i. e. at around 40 m depth in the innermost stations

temperature rise from 1.5 to 2 ˚C occurs simultaneously with the change of salinity gradient from 31.5 to 32). All in all, the salinity gradient below 10 m was similar at the middle and innermost stations.

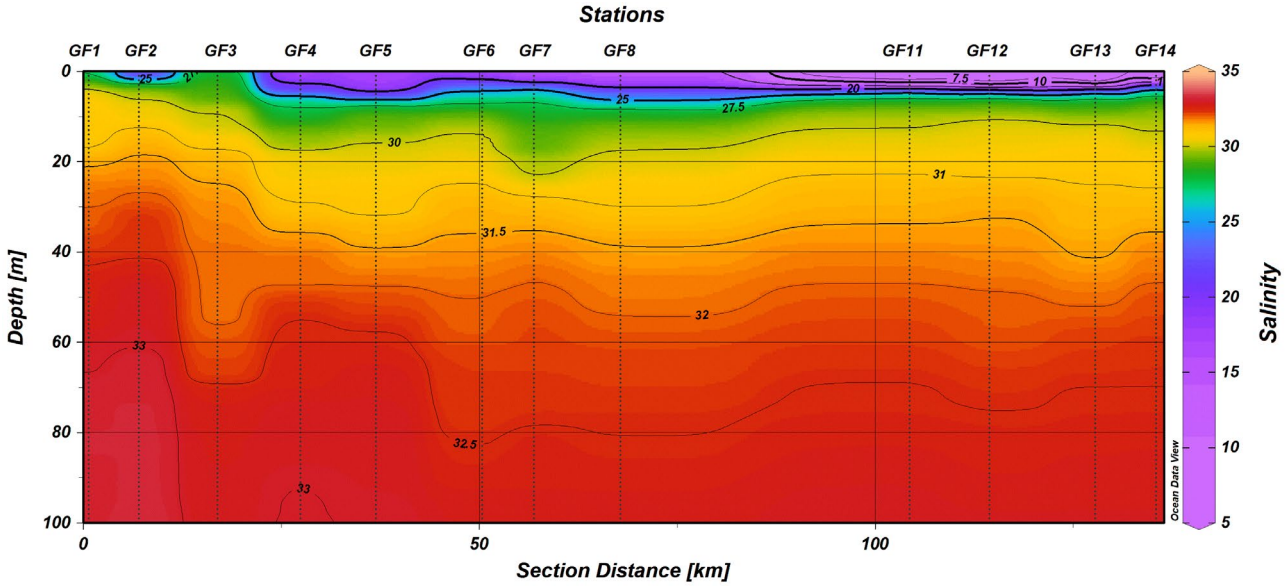

Figure 3 Salinity in the upper 100 m along the fjord transect. Datapoints are from every 1 m shown as vertical dotted lines.

5.1.3 Irradiance

The irradiance surface values at the sampled stations varied driven by cloudiness and direct sunlight (Figure 4). The depth of the photic zone varied between 12 m (GF14 and GF11) and 31 m (at GF3). The second deepest photic zone was found at GF12 (21 m) and third deepest at GF6 (19 m). Average depth of the euphotic zone was 17 meters.

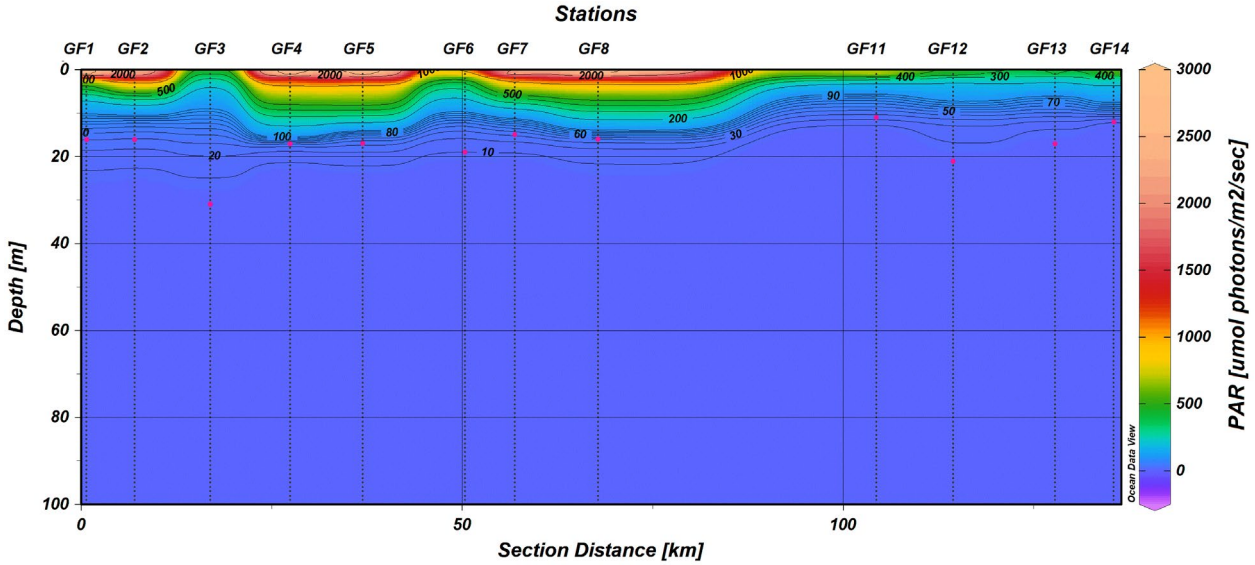

Figure 4 Irradiance in the PAR spectrum along the fjord transect. Datapoints are from every 1 m shown as vertical dotted lines. Red points represent the depth of the photic zone (1% surface value).

5.2 Nutrients

5.2.1 Phosphate

Phosphate concentrations in the IF were low in the surface and high in the deeper water column (Figure 5). This vertical concentration gradient weakened towards the OF. Phosphate concentrations varied from 0.08 µM at GF7 (5 m) to 0.74 µM at GF14 (100 m). Within the water column phosphate concentrations were stratified at all stations with relatively low concentration in the surface layers excluding GF1 where surface values were more than 0.36 µM and GF3 where the lowest concentration was found from the depth of 10 meters (0.32 µM). Low phosphate concentrations (< 0.3 µM) were clearly linked to low salinity (S ≥ 30) surface water excluding GF5, where the phosphate level was relatively high (0.4 µM).

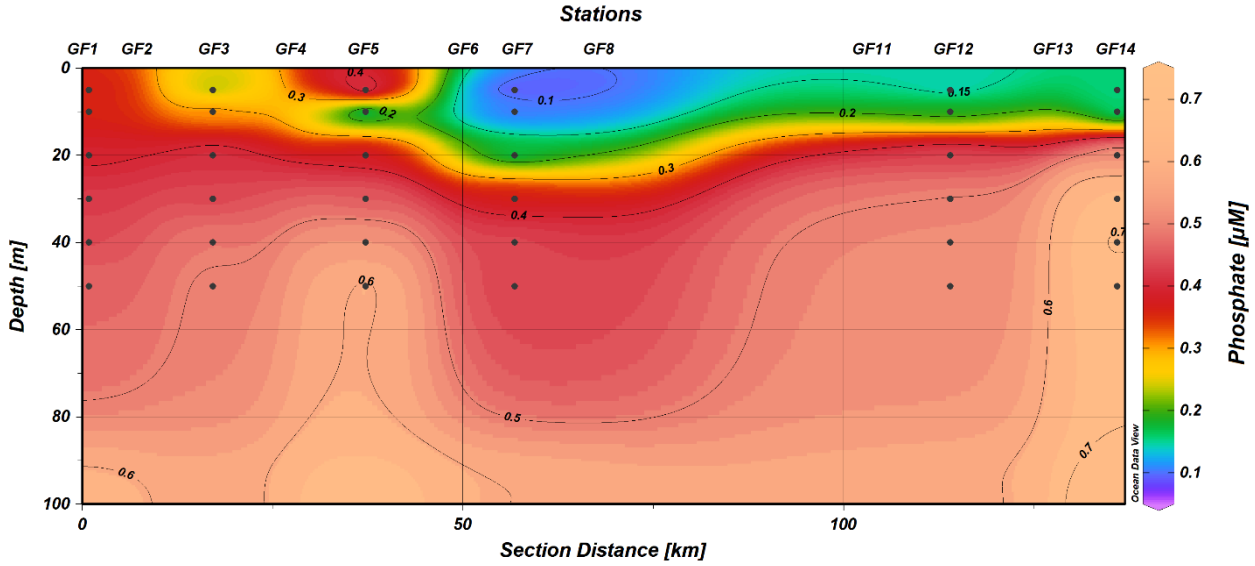

Figure 5 Phosphate concentrations along the fjord transect. Dots represent sampling depths at each station.

5.2.2 Silicate

Silicate concentration varied greatly, also between nearest stations (Figure 6). The lowest values of silicate for each station were found at ca. 20 m depth. The overall highest silicate concentration of 8.8 µM was found together with the relatively high phosphate concentration from the surface water at GF5 (5 m). Silicate concentrations were also high at GF14 throughout the water column whereas at GF1 they were relatively low. Silicate concentrations at GF12 were below the detection limit. Often low silicate concentrations (≤ 1 µM) occurred together with cold water temperatures (T ≤ 2˚C)

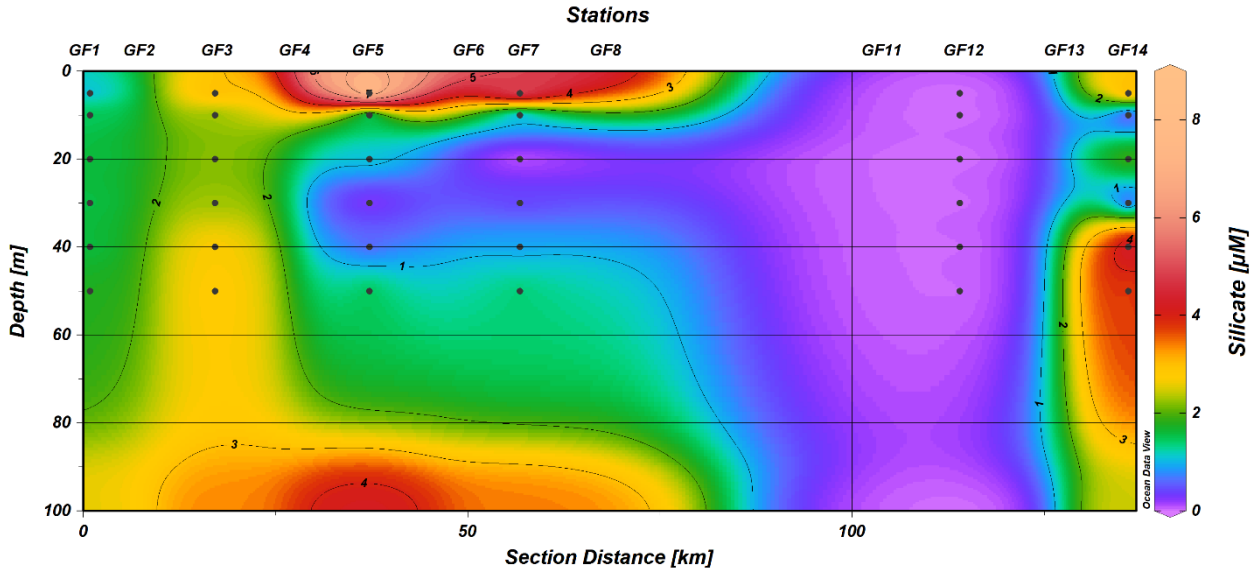

Figure 6 Silicate concentrations along the fjord transect. Dots represent sampling depths at each station.

5.2.3 Dissolved inorganic nitrogen

The sum of dissolved inorganic nitrite and nitrate (NOx) concentrations was higher in the IF than OF. Low NOx concentrations were often detected combined with warm water temperatures (T ≥ 3.0 ˚C). At the middle stations and innermost stations high concentrations coincided with more saline water (S ≥ 30.0). Surface values were low at all stations. NOx was depleted at each station in 5 m depth except of GF3 where it was depleted at 20 m.

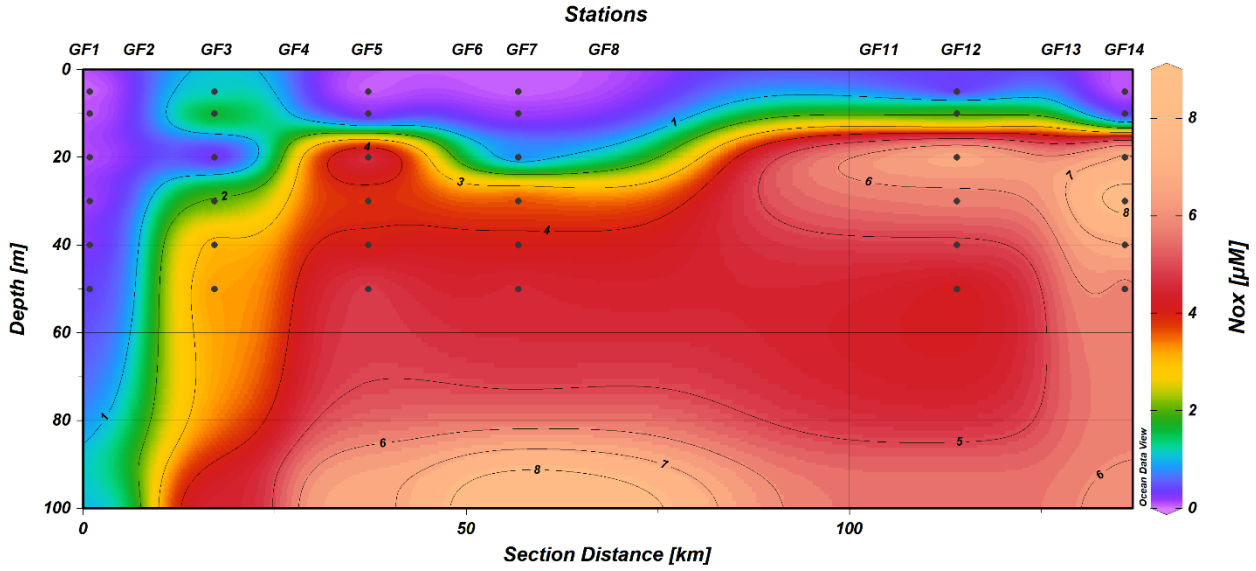

Figure 7. NOx concentrations along the fjord transect. Dots represent sampling depths at each station.

5.2.4 Nutrient ratios

Based on Redfield-Brzezinski ratio (Brzezinski 1985; Redfield 1934, 1958; Table 3) phosphate was never the potentially limiting nutrient even though values at e.g. GF7 were very low (Figure 5). At all stations phytoplankton growth was potentially nitrogen (sum of dissolved nitrate and nitrite) limited in the surface water and in addition at GF1 until 100 m and at GF 3 until 30 m as the calculated N:Si ratio was below the Redfield- Brzezinski ratio of 1.067. The same pattern of very low nitrogen concentration was seen in the nitrogen contour plot (Figure 7). All the other stations had relatively high nitrogen concentrations in the deeper water column whereas at GF1 and GF3 nitrogen concentration remained under 4.5 µM. At all stations excluding GF1 silicate was the potentially limiting nutrient in the deeper water layers.

Nevertheless, it should be noted that in the deeper water column phytoplankton was limited by light rather than nutrients (Figure 4).

Table 3 Relative nutrient limitation between dissolved inorganic nitrogen and silicate based on the Redfield-Brzezinski ratio. Cells with red color indicate potential N limitation, those with blue color Si limitation.

Ratio N:Si (16:15≈1.067)						
Depth (m)	GF1	GF3	GF5	GF7	GF12	GF14
5	0:0.97	0.34	0:8.91	0:5.78	0:0	0:3.56
10	0.03	0.88	0:0.20	0.7	2.07:0	0:0
20	0.05	0:2.21	4.5	0.48:0	7.21:0	3.62
30	0.05	0.9	34.46	10.63	5.87:0	8.74:0
40	0.08	1.18	9.89	4.64	4.97:0	1.41
50	0.21	1.19	3.00	3.1	3.93:0	1.49
100	0.38	1.33	1.63	2.54	5.61:0	2.48

N < Ratio

Si < Ratio

5.2.4 Relationship of physical and chemical variables and grouping of stations

Principal Component Analysis (PCA) was performed with the physical and chemicals variables NOx, silicate, phosphate, temperature, salinity, depth and distance from NS. These variables explained 71.5% of the total variance in the data (Figure 8). Dimension 1 was mainly explained by NOx (25.0%) followed by phosphate, salinity and depth (Figure 9A), and Dimension 2 by temperature (30.6%) followed by distance and silicate (Figure 9B). Temperature and distance were aligned in the negative corner of Dimension 1 and 2. Depth and phosphate aligned towards the bottom right corner in the positive side of Dimension 1.

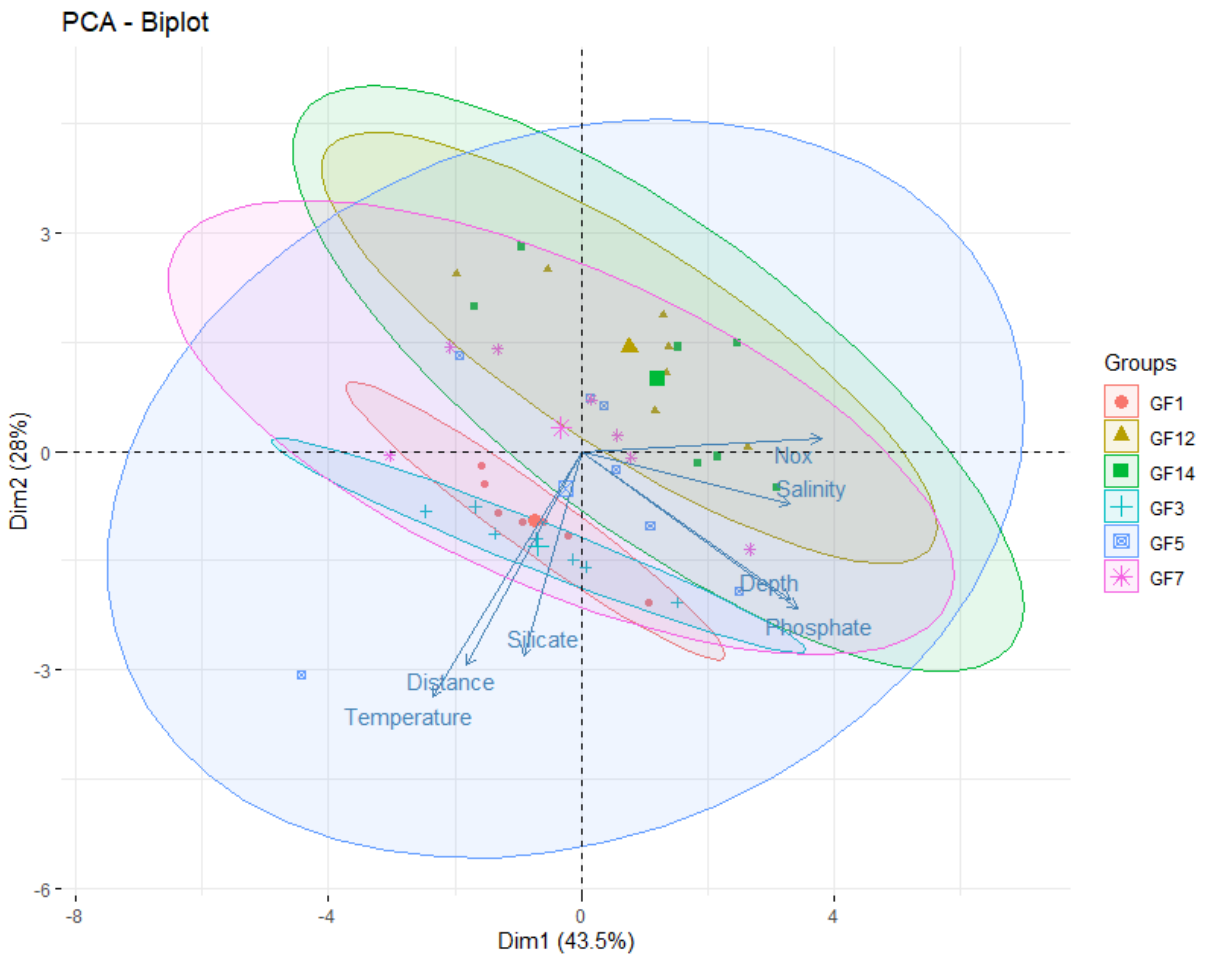

Figure 8 PCA biplot showing the correlations of physical parameters (NOx, silicate, phosphate, temperature, salinity, depth and distance from glaciers) between single samples (i. e. individual depth at each station). Ellipses encompass the observations from each station. Arrows indicate the contribution of certain environmental variables to the grouping – the longer the arrow, the stronger the influence.

PCA Biplot shows a clear separation of innermost and outermost stations, and middle stations were characterized by greater variability of environmental conditions (Figure 8). GF1 and GF3 were plotted into the bottom-left section linked to the direction of temperature, distance from glacier and salinity, where as GF12 and GF14 were in the upper-right corner in the opposite direction. The middle station GF5 and GF7 were mainly located in-between the innermost and outermost stations except for GF5 5 m, which was found from the bottom left corner and GF7 10 m, which was located in between the outermost stations.

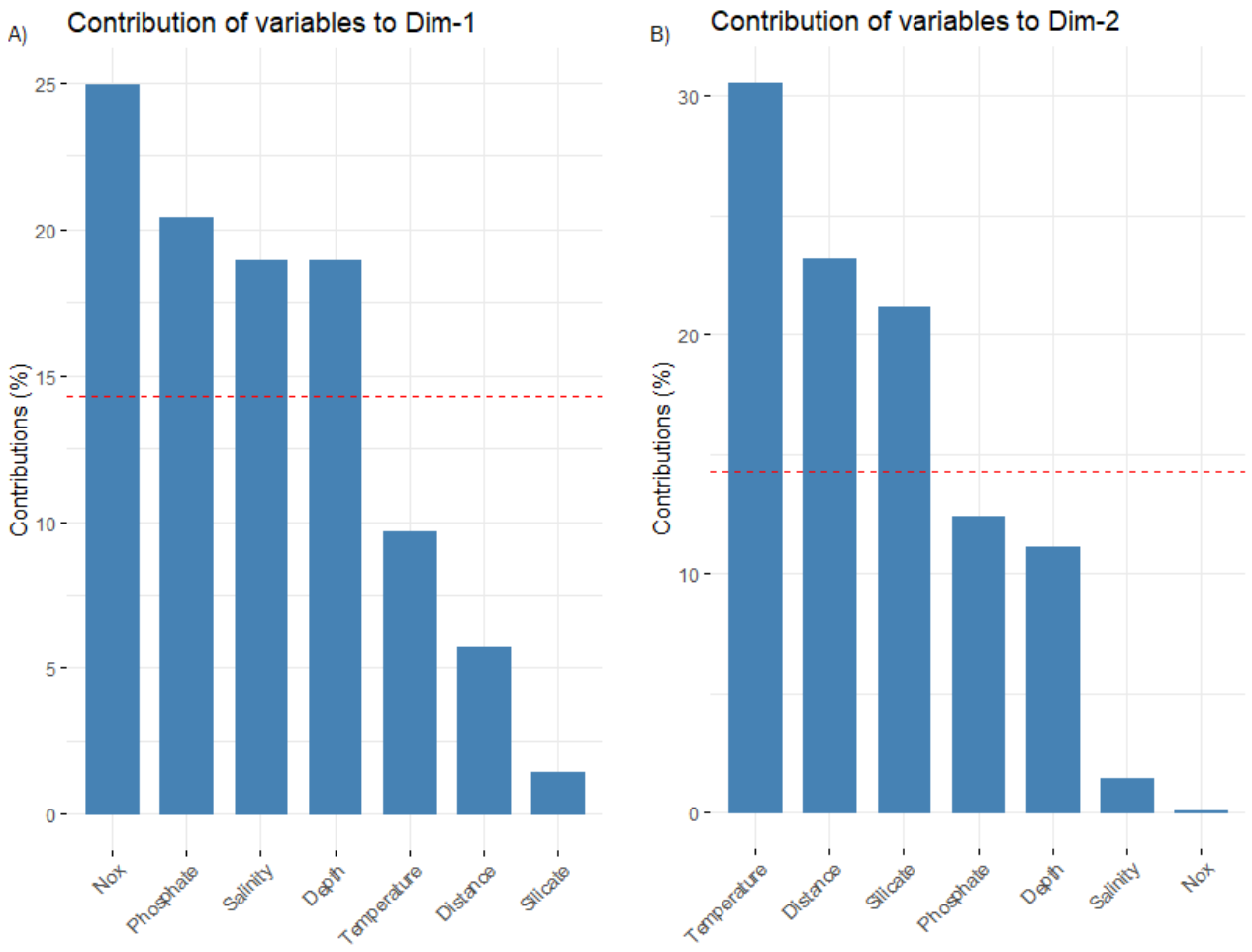

Figure 9 Relative contribution of variables to A) Dimension 1 and B) Dimension 2.

5.3 *In situ* fluorescence and chlorophyll *a*

All stations had clear subsurface fluorescence maxima in 10 to 20 m depth while surface and deep values were low (Figure 10). Fluorescence values were higher in the IF than OF (Figure 10). Innermost stations had the highest values in a thin layer whereas at the middle stations algal chlorophyll was vertically wider and more evenly distributed. In the OF and especially at GF3 fluorescence values were low although at GF3 chl *a* fluorescence value remained over 0.5 µg/l until 65 m. The by far highest (41.6 µg/l) and the lowest (0.1 µg/l) fluorescence values were measured at GF14. Other stations with high fluorescence peaks were GF11 at 13 m (29.6 µg/l), GF8 at 14 m (9.1 µg/l), and GF4 at 23 m (9.5 µg/l).

Overall, the extracted chl *a* values were lower than estimates based on florescence measurements (Figure 11 and Figure 12). In most stations chl *a* measurement followed

fluorescence reasonably well (Figure 12, for example GF5-GF7), even within a small-scale variability (Figure 12, GF3) whereas at some stations there were clear differences between the two methods (Figure 12, GF14). At some stations chl *a* sampling from selected water depths resulted in missing the chl *a* maximum (Figure 12, GF8) whereas at GF12 10 m sample captured the chl *a* peak seen in the fluorescence measurements. This is also shown from the contour plot (Figure 11).

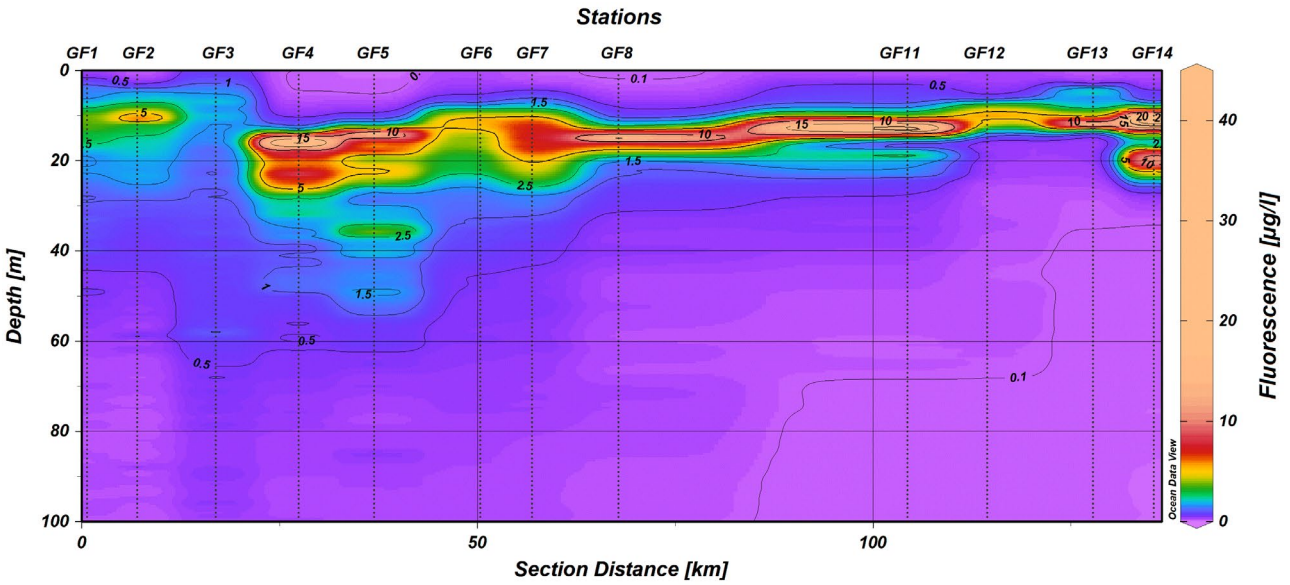

Figure 10 Algal chlorophyll fluorescence along the fjord transect. Datapoints are from every 1 m shown as vertical dotted lines.

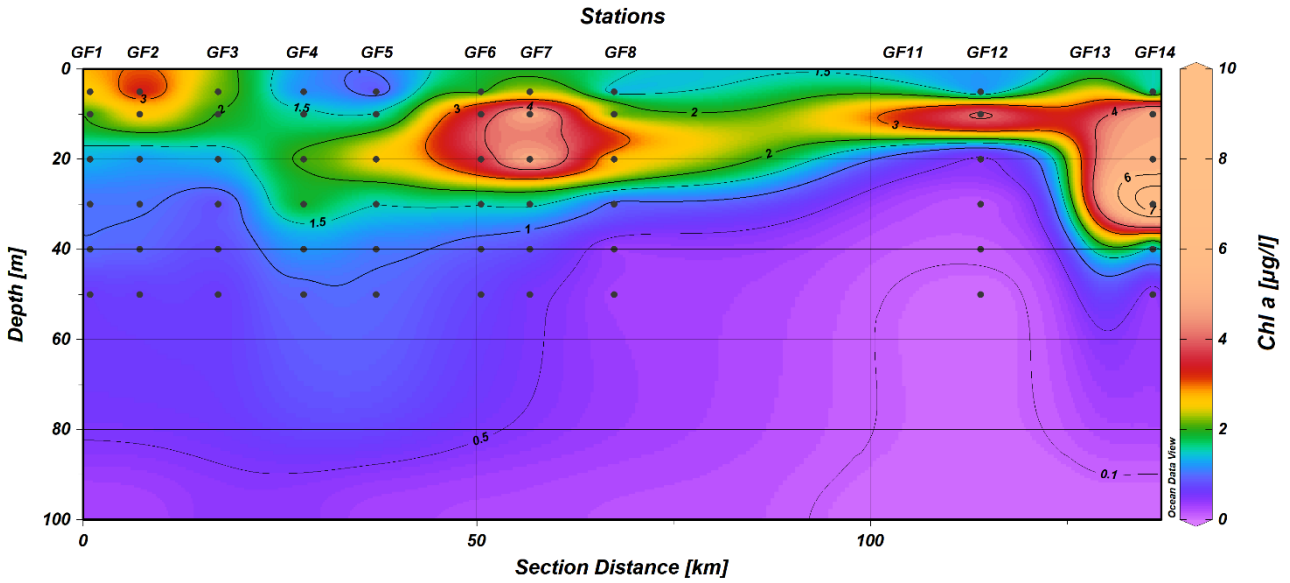

Figure 11 Chlorophyll *a* concentrations along the fjord transect. Dots represent sampling depths at each station.

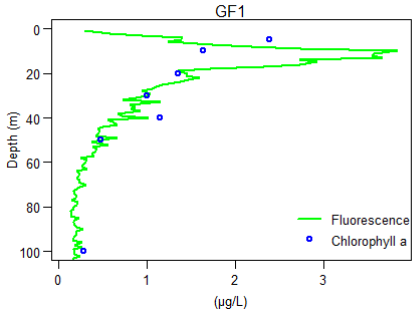
GF1
Depth (m)
0
20
40
60
80
100
0
1
2
3
(µg/L)
Fluorescence
Chlorophyll a

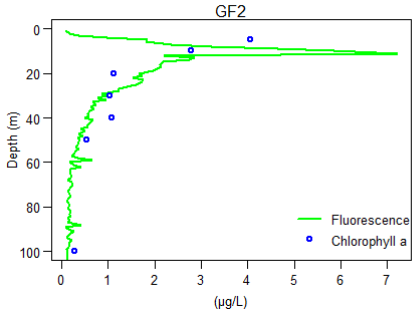
GF2
Depth (m)
0
20
40
60
80
100
0
1
2
3
4
5
6
7
(µg/L)
Fluorescence
Chlorophyll a

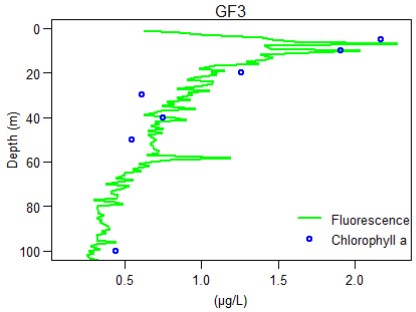
GF3
Depth (m)
0
20
40
60
80
100
0.5
1.0
1.5
2.0
(µg/L)
Fluorescence
Chlorophyll a

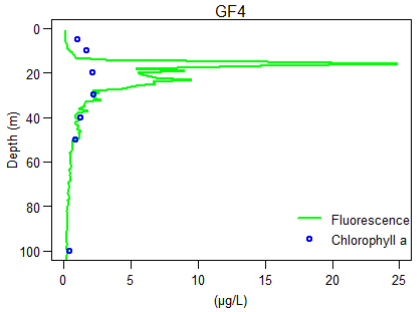
GF4
Depth (m)
0
20
40
60
80
100
0
5
10
15
20
25
(µg/L)
Fluorescence
Chlorophyll a

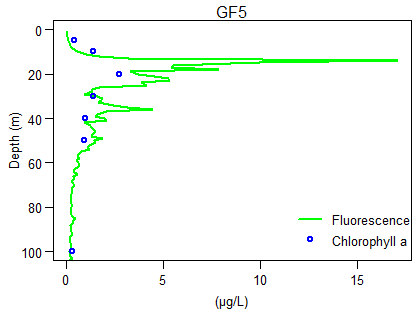
GF5
Depth (m)
0
20
40
60
80
100
0
5
10
15
(µg/L)
Fluorescence
Chlorophyll a

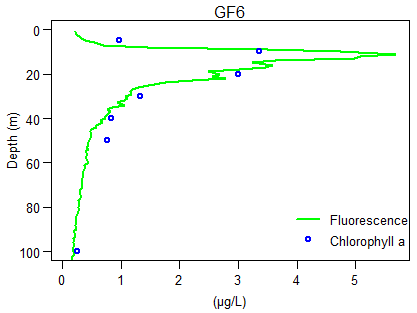
GF6
Depth (m)
0
20
40
60
80
100
0
1
2
3
4
5
(µg/L)
Fluorescence
Chlorophyll a

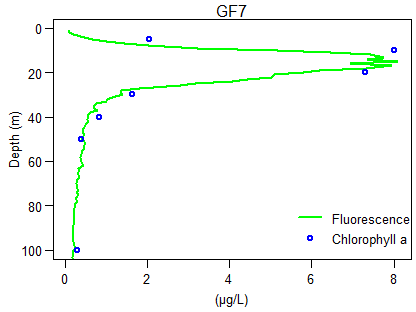
GF7
Depth (m)
0
20
40
60
80
100
0
2
4
6
8
(µg/L)
Fluorescence
Chlorophyll a

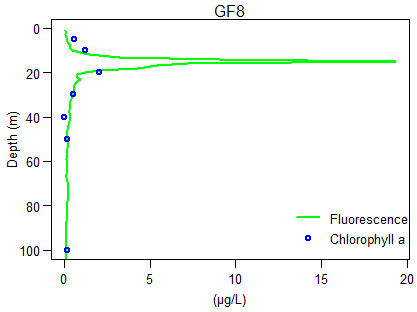
GF8
Depth (m)
0
20
40
60
80
100
0
5
10
15
20
(µg/L)
Fluorescence
Chlorophyll a

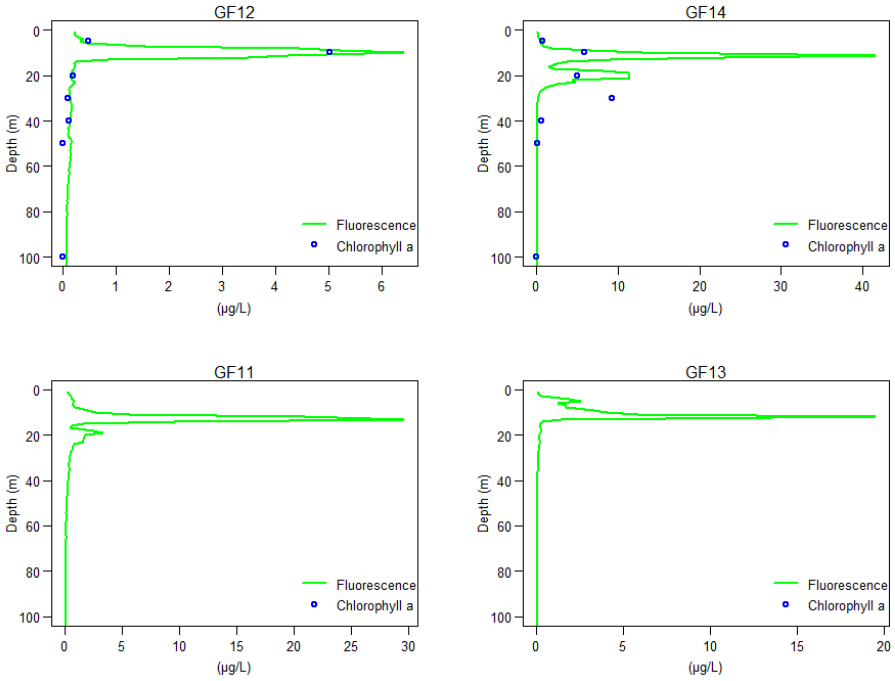

Figure 12 Vertical distribution of algal fluorescence (green lines) data from CTD sensor at all stations and extracted chlorophyll *a* analyses (blue dots) at all stations excluding GF11 and GF13.

A significant linear regression was found between chl *a* concentrations and extracted PCA Dimension 1 (Table 4, Figure 13). Estimated model fit (beta-coefficient) between Dimension 1 and chl *a* was -0.51 with standard error of 0.15 and significant level of $p < .01$. The model fit was $F=6.472$, $df=39$ and $p = .004$. Linear regression between chl *a* and Dimension 2 was not significant (Table 6). The model without interaction was chosen based on the results of model comparison (ANOVA, $p > .05$) aiming for a simpler model.

Table 4 Beta coefficient, Standard Error (SE), *p*-value, *F*-Statistic (F), Degrees of freedom (DF) and P-value of regression models between extracted PCA Dimensions 1 (PC1) and 2 (PC2) and chl *a* concentrations with interaction (Model 1) and with additive model (Model 2).

	Beta coefficient	**SE**	***p*-value**	***F***	**DF**	**P-value**
Model 1				4.47	38	**0.009**
PC1	-0.54	0.16	**0.002**			
PC2	0.21	0.20	0.29			
Interaction	-0.08	0.10	0.45			
Model 2				6.47	39	**0.004**
PC1	-0.51	0.15	**0.002**			
PC2	0.26	0.19	0.19			

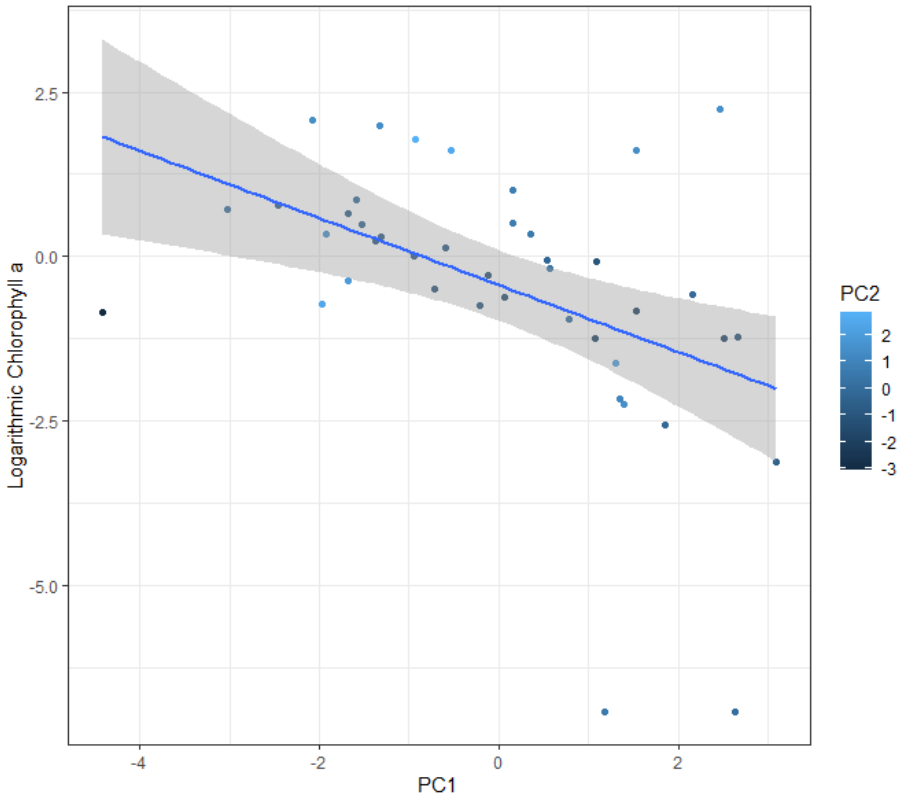

Figure 13 Chlorophyll *a* and PCA Dimension 1 had significant linear relationship.

5.4 Phytoplankton

5.4.1 Species abundance and community composition

Phytoplankton abundances decreased from the IF towards the OF (Figure 14). Phytoplankton was most abundant at the depth of 20 m at GF5, GF7 and GF14. Phytoplankton was most abundant at 20 m at GF14 whereas the lowest abundances were found at the same station from the depth of 5 m and 40 m. Cell counts at GF14 20 m were four times higher than in the second abundant sample from GF7 20 m. In GF12 cell abundances were low at all depths. In all the other stations, there was one depth having more than double the concentration of the cells compared to the second abundant depth indicating clear abundance maxima as also seen in algal fluorescence (Figure 10). Average abundances of cells per specific phytoplankton groups are shown below (Table 5).

Table 5 Average abundance of phytoplankton groups and the average total abundance in Godthåbsfjord long-transact. All the groups do not include groups listed before them (e. g. group *Chaetoceros* spp. excludes *Chaetoceros socialis*). Statistics of the group *Chaetoceros socialis* was mainly dominated by sample GF14 20 m and when excluded the average abundance was 1205693 cells/l and standard deviation 1816355 cells/l.

Phytoplankton group	Average abundance (cells/l)	Standard deviation (cells/l)
Chaetoceros socialis	2674821	6309326
Chaetoceros spp.	108476	120343
Other diatoms	18810	15158
Dinoflagellates	7060	6901
Dinobryon balticum	68883	103548
Other flagellates	34390	64454
Other taxa	41798	67292
TOTAL	2954238	6307698

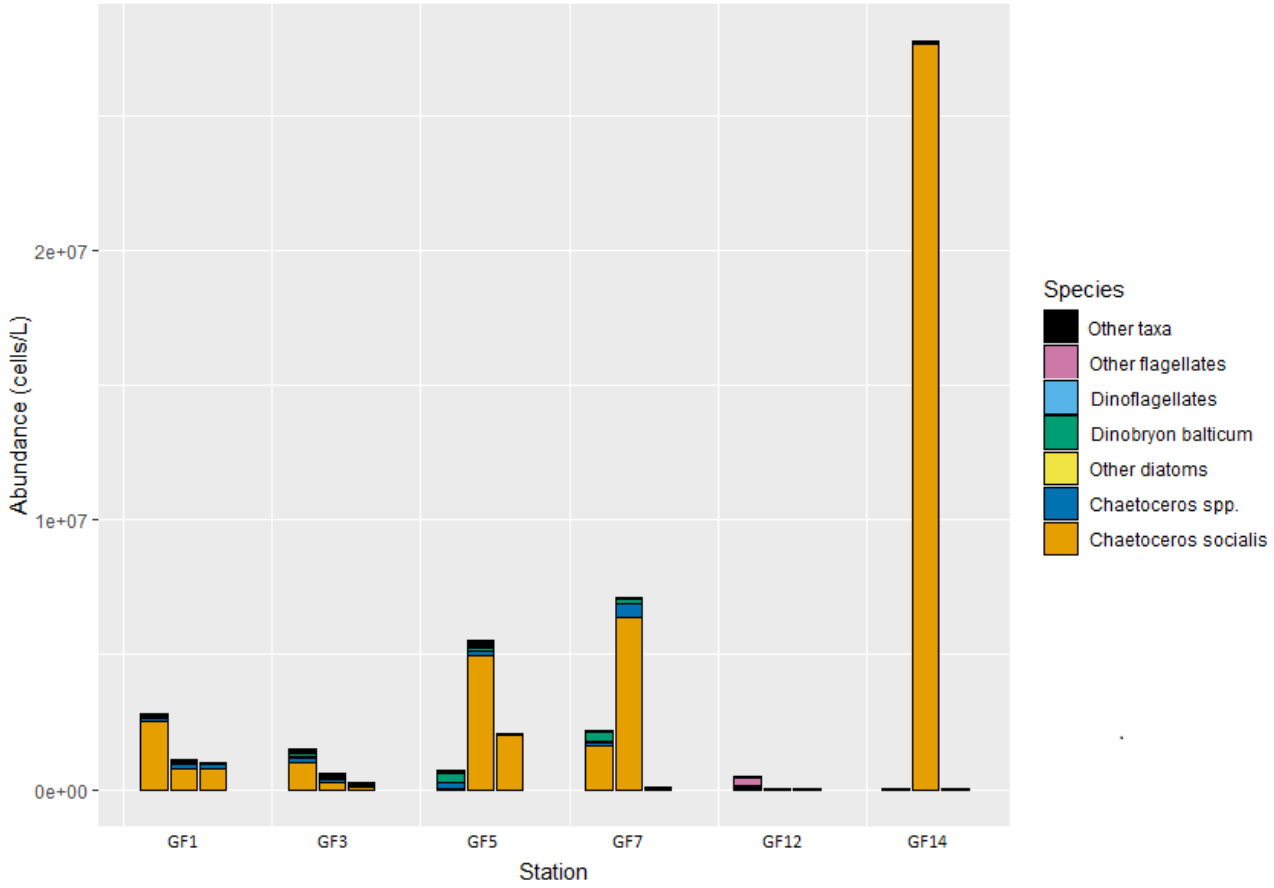

Figure 14 Algal abundance per sample. At each station the first bar on the left is 5 m, middle bar is 20 m and the right one is 40 m depth.

Chaetoceros socialis was the most abundant species dominating phytoplankton community in each sample, except GF5, GF12 and GF14 at 5 m depth, and GF12 and GF14 at 40 m depth (Figure 15). Dinoflagellates were the dominating group (54%) at GF14 5 m. However, cell counts in this station were low, so dnoflagellate abundances were also low compared to the other stations. *Chaetoceros* species excluding *C. socialis* were the dominating group in GF12 40 m (45% but again cell counts in the sample were low). At GF 5 5 m phytoplankton community was dominated by *Dinobryon balticum* (46%) followed by *Chaetoceros* species other than *C. socialis* (36%). At GF12 5 m phytoplankton community was dominated by unidentified flagellates and GF14 40 m had the most evenly distributed community between all seven defined groups (Figure 15). The complete list of all the phytoplankton species is seen as an Appendix 1.

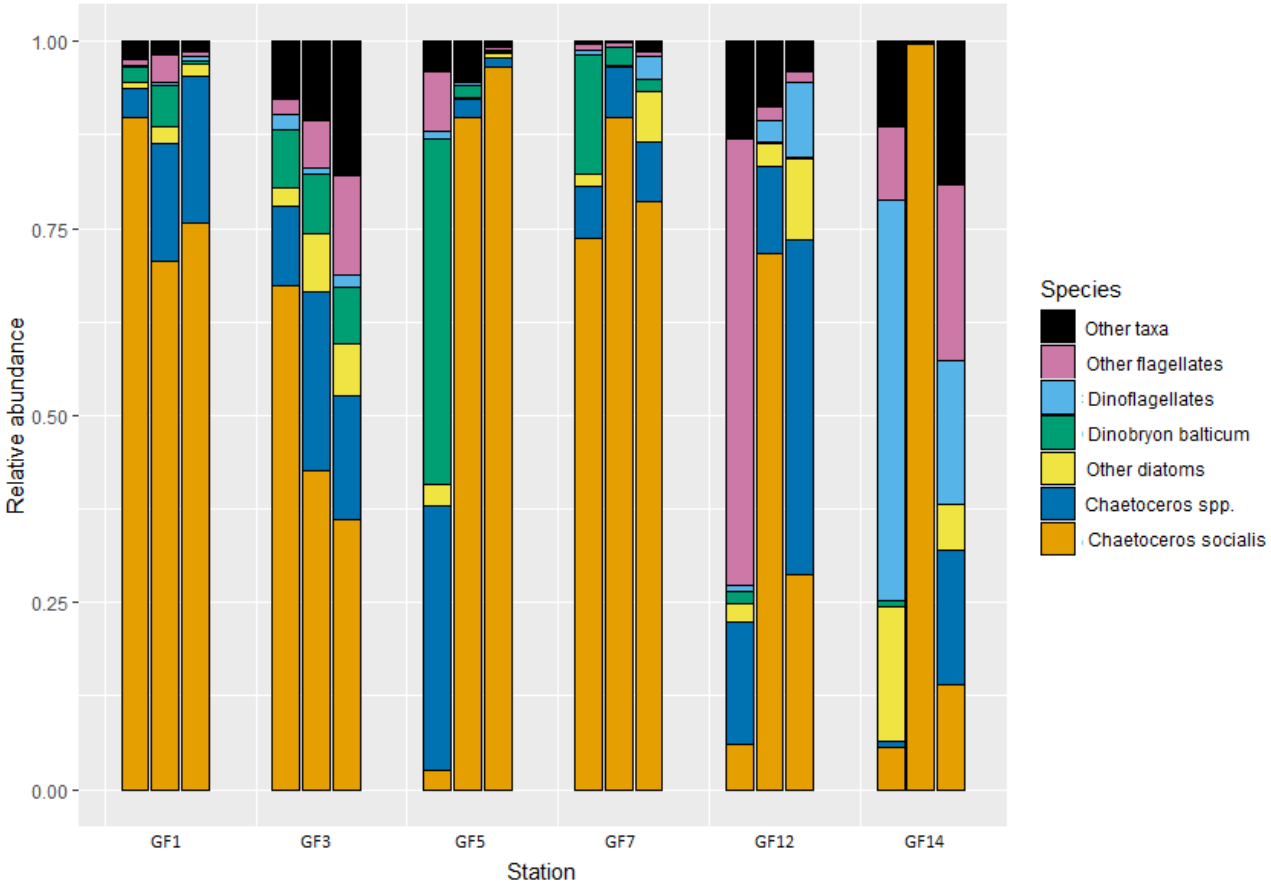

Figure 15 Relative species abundance per sample. At each station the first bar on the left is 5 m, middle bar is 20 m and the right one is 40 m depth.

In general, species richness (Figure 16) was lower near the glacier and increased towards the outermost stations. In the outermost stations GF1, GF3 and GF5 species richness was highest at 5 m depth, whereas in the innermost stations the highest values were discovered at the dept of 20 m (GF7 and GF12) or 40 m (GF14). Lowest richness values occurred at the stations GF12 and GF14. GF14 20 m had only 12 different species which was four species less than in the second poorest sample at 5 m also from GF14. The highest species richness was found from GF7 20 m with 43 species followed by GF3 5 m with 41 species.

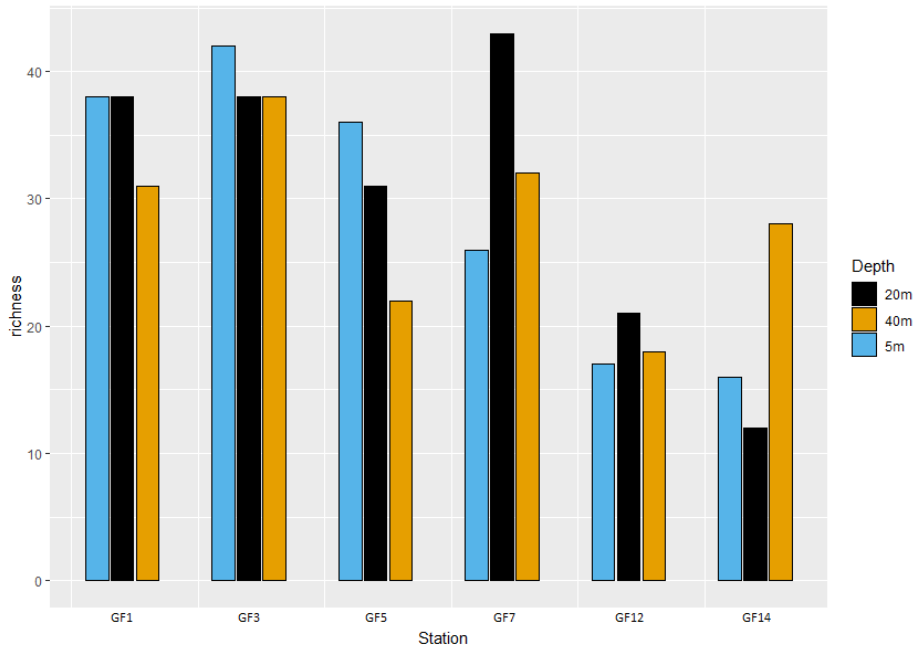

Figure 16 Species richness per sample. At each station the first bar on the left is 5 m, middle bar is 20 m and the right one is 40 m depth.

At GF7, GF12 and GF14 the lowest effective number of species (ENS, Figure 17) was found at 20 m depth. At GF1 ENS was highest in 20 m (1.94), but still relatively low compared to highest values at the other stations. The lowest ENS was found from GF14 20 m (1.01) whereas the highest values were from the remaining depths at the same station (GF14 40 m 9.25 and GF14 5 m 7.09). The same patterns were observed for Shannon's and Pielou's diversity indices (Figure 18 and 18).

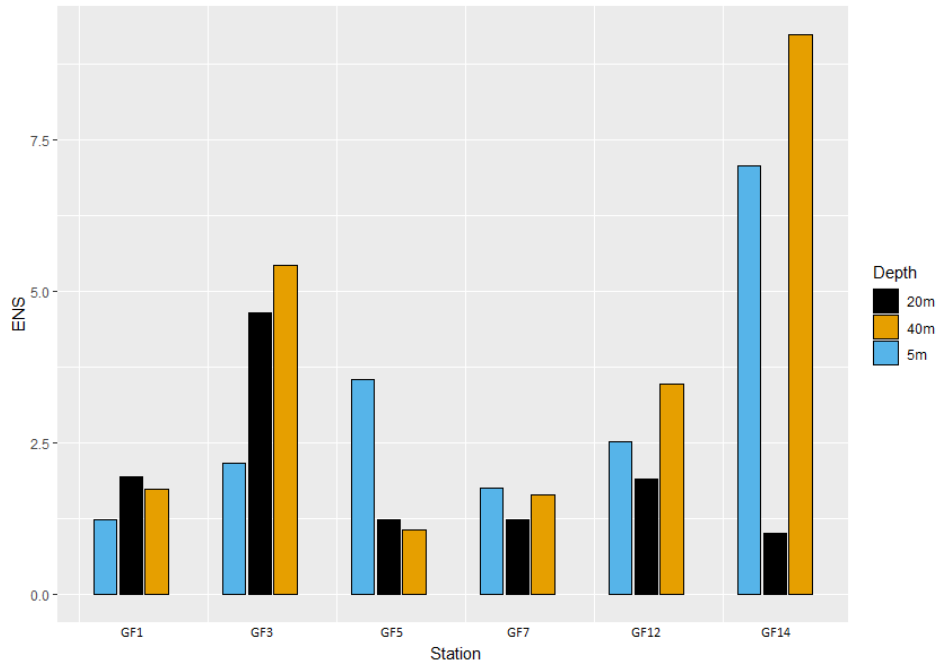

Figure 17 Effective number of species per sample. At each station the first bar on the left is 5 m, middle bar is 20 m and the right one is 40 m depth.

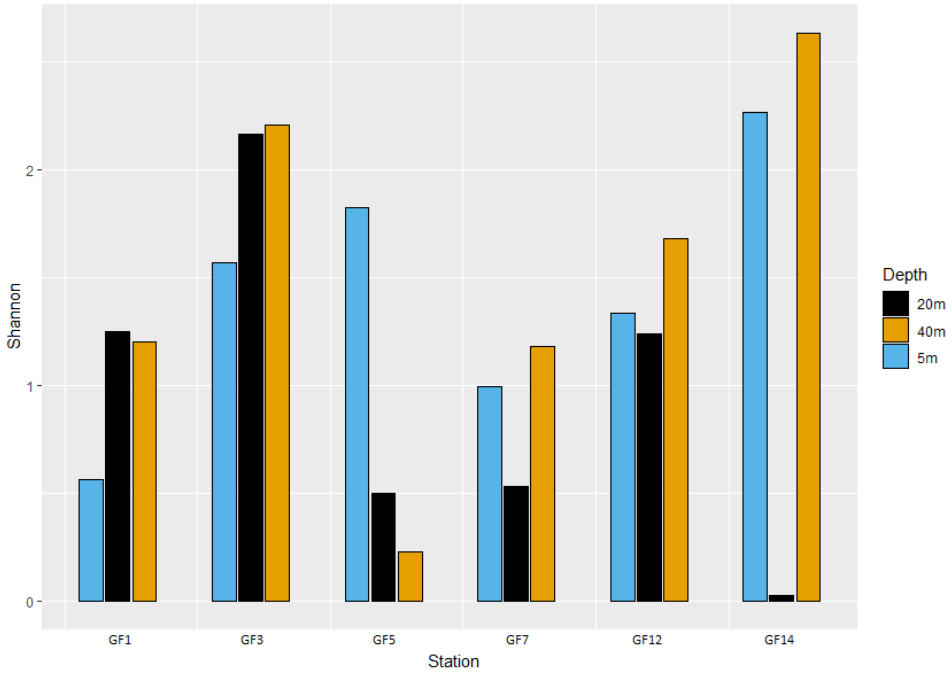

Figure 18 Shannon's diversity index per sample. At each station the first bar on the left is 5 m, middle bar is 20 m and the right one is 40 m depth.

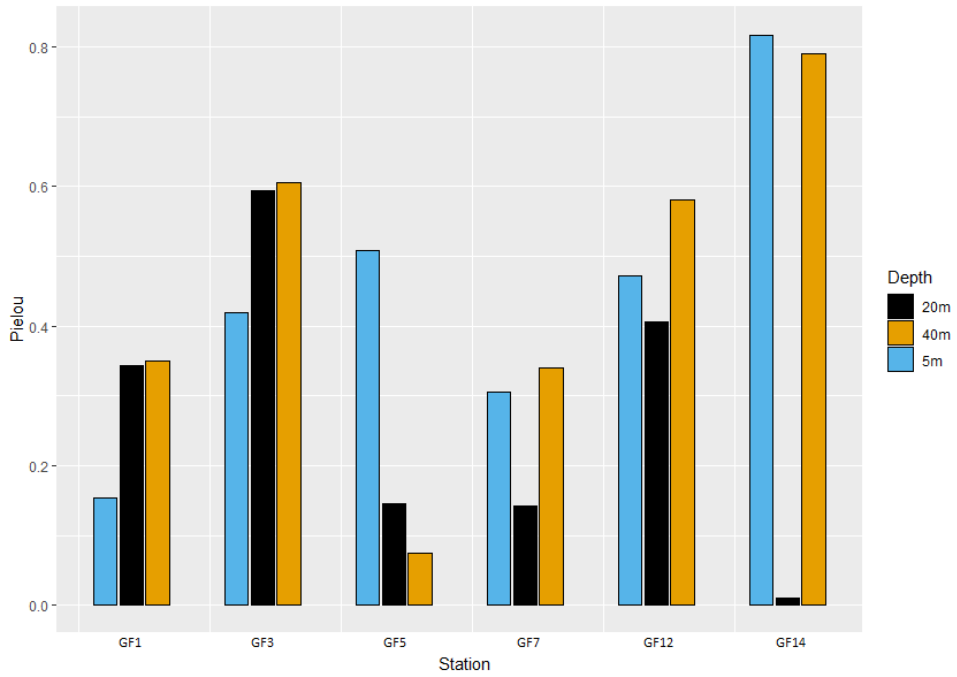

Figure 19 Pielou's evenness index per sample. In samples with high values algal cells are more evenly distributed across different species, whereas samples with low values are highly dominated by one or few species. At each station the first bar on the left is 5 m, middle bar is 20 m and the right one is 40 m depth.

Phytoplankton cell counts and chlorophyll a concentrations were strongly correlated (Figure 20, $r = 0.78$, $p < .001$). The 20 m sample from GF14 containing high abundances was considered as an outlier (Cook's distance > 1) and was therefore removed from the analysis.

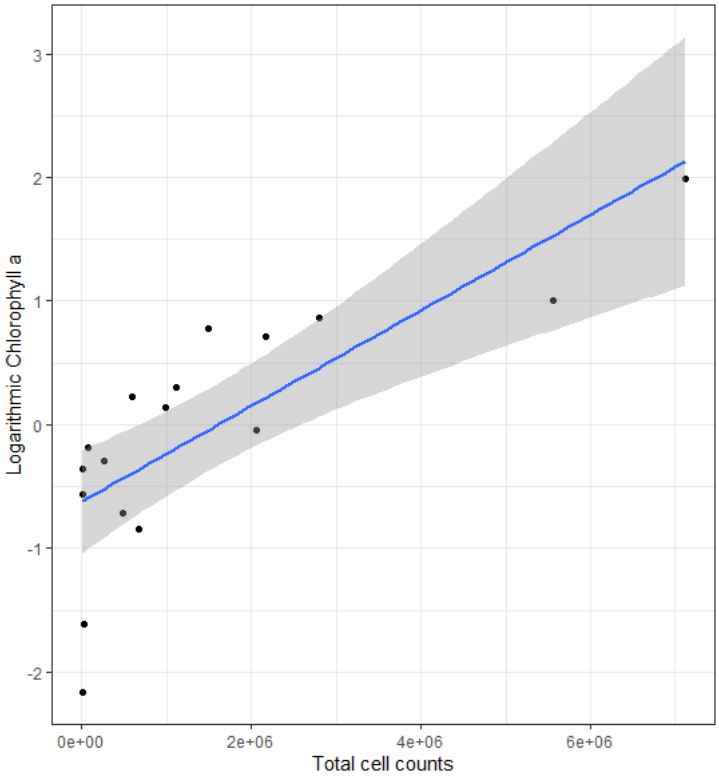

Figure 20 A simple correlation between logarithmic chlorophyll *a* and total cell counts

A significant negative linear regression was found between logarithmic chl *a* concentrations and Pielou's evenness index (Table 6, Figure 21). Also, there was a significant positive linear regression between logarithmic chl *a* and species richness (Table 6, Figure 22). In the later model the sample from GF14 20 m containing low species richness was considered as an outlier (Cook's distance > 1) and was therefore removed from the analysis.

Table 6 Beta coefficient, Standard Error (SE), *p*-value, *F*-Statistic (F), Degrees of freedom (DF) and P-value of a linear regression model between Pielou's evenness index (explanatory variable) and logarithmic Chlorophyll *a* (response variable) as Model 1 and a linear regression model between species richness (explanatory variable) and logarithmic Chlorophyll *a* (response variable) as Model 2

	Beta coefficient	**SE**	***p*-value**	***F***	**DF**	**P-value**
Model 1	-2.80	0.88	**0.006**	10.18	16	**0.006**
Model 2	0.07	0.02	**0.005**	11.06	15	**0.005**

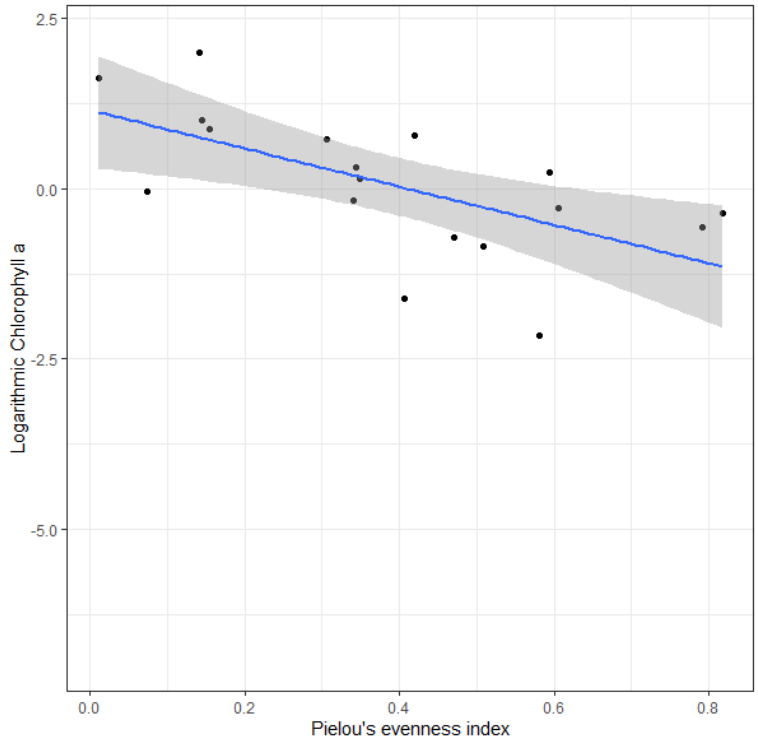

Figure 21 A linear regression line between logarithmic Chlorophyll *a* and Pielou's evenness index

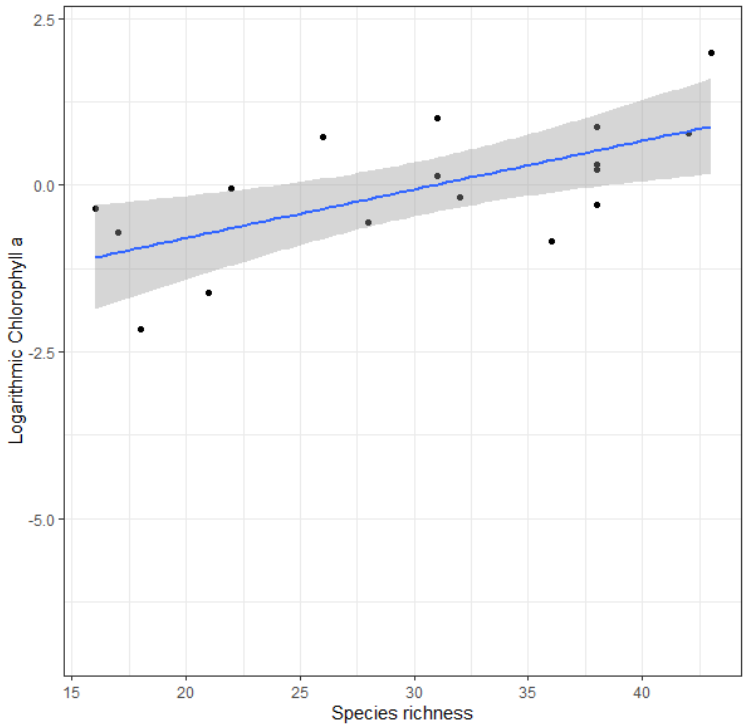

Figure 22 A linear regression line between logarithmic Chlorophyll *a* and species richness evenness index

Also, there was a significant linear relationship between species richness (the number of species) and Dimension 2 (Table 7, Figure 23). Estimated model fit (beta-coefficient) between Dimension 2 and richness was -3.89 with standard error of 1.44 and significant level of $p < .05$. The model fit was F = 5.89, df = 15 and $p = .01$. Linear regression between richness and Dimension 1 was not significant (Table 7). The model without interaction was chosen based on the results of model comparison (ANOVA, p > .05) aiming for a simpler model. A linear regression was not found between Dimensions 1 and/or 2 and any other diversity indices including the effective number of species (ENS), the Shannon's diversity index and Pielou's evenness index.

Table 7 Beta coefficient, Standard Error (SE), *p*-value, *F*-Statistic (F), Degrees of freedom (DF) and P-value of regression models between extracted PCA Dimensions 1 (PC1) and 2 (PC2) and chl *a* concentrations with interaction (Model 1) and without interaction (Model 2).

	Beta coefficient	**SE**	***p*-value**	**F**	**DF**	**P-value**
Model 1				4.88	14	0.02
PC1	-1.09	1.13	0.35			
PC2	-5.54	1.82	**0.009**			
Interaction	-0.96	0.67	0.18			
Model 2				7.73	15	**0.01**
PC1	-1.01	1.16	0.40			
PC2	-3.88	1.44	**0.02**			

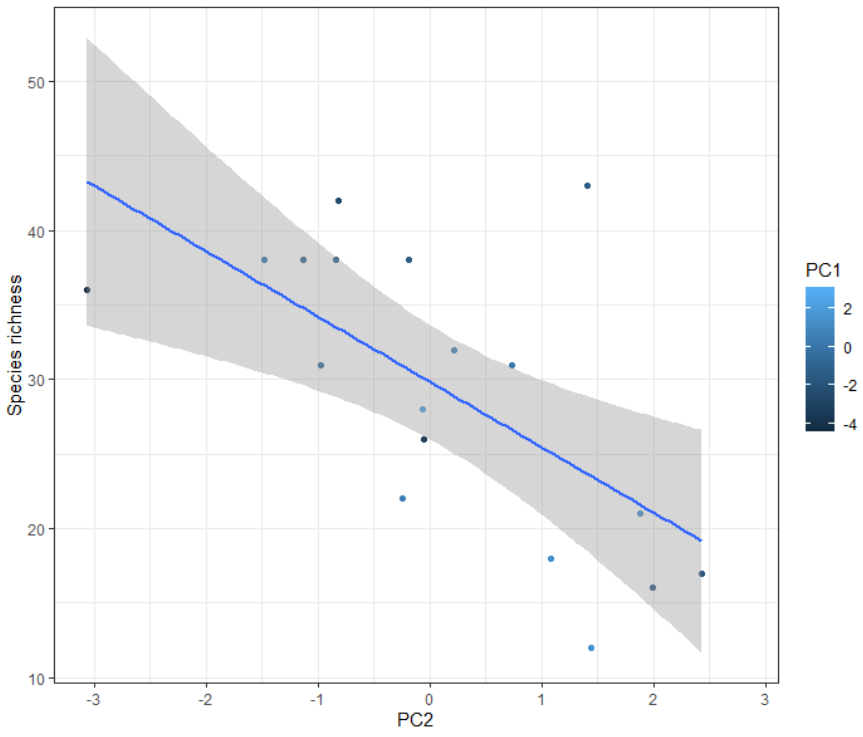

Figure 23 Species richness and PCA Dimension 2 had a significant monotonic relationship.

4.5.2 Similarity of species composition

Multidimensional scaling and cluster analysis showed some week clustering with Jaccard similarity index but not with Bray-Curtis similarity index. Multidimensional scaling (Figure 24 D) with Jaccard similarity index showed a separation of stations according to location. The outermost stations GF1 and GF3 were located on the left side of the x-axis, followed by middle stations GF5 and GF7 and the innermost stations GF12 and GF14 were located on the right side of the x-axis. The separation within the MDS -plots based on Bray-Curtis similarity was more complex but still separated stations and/or regions (Figure 24 C).

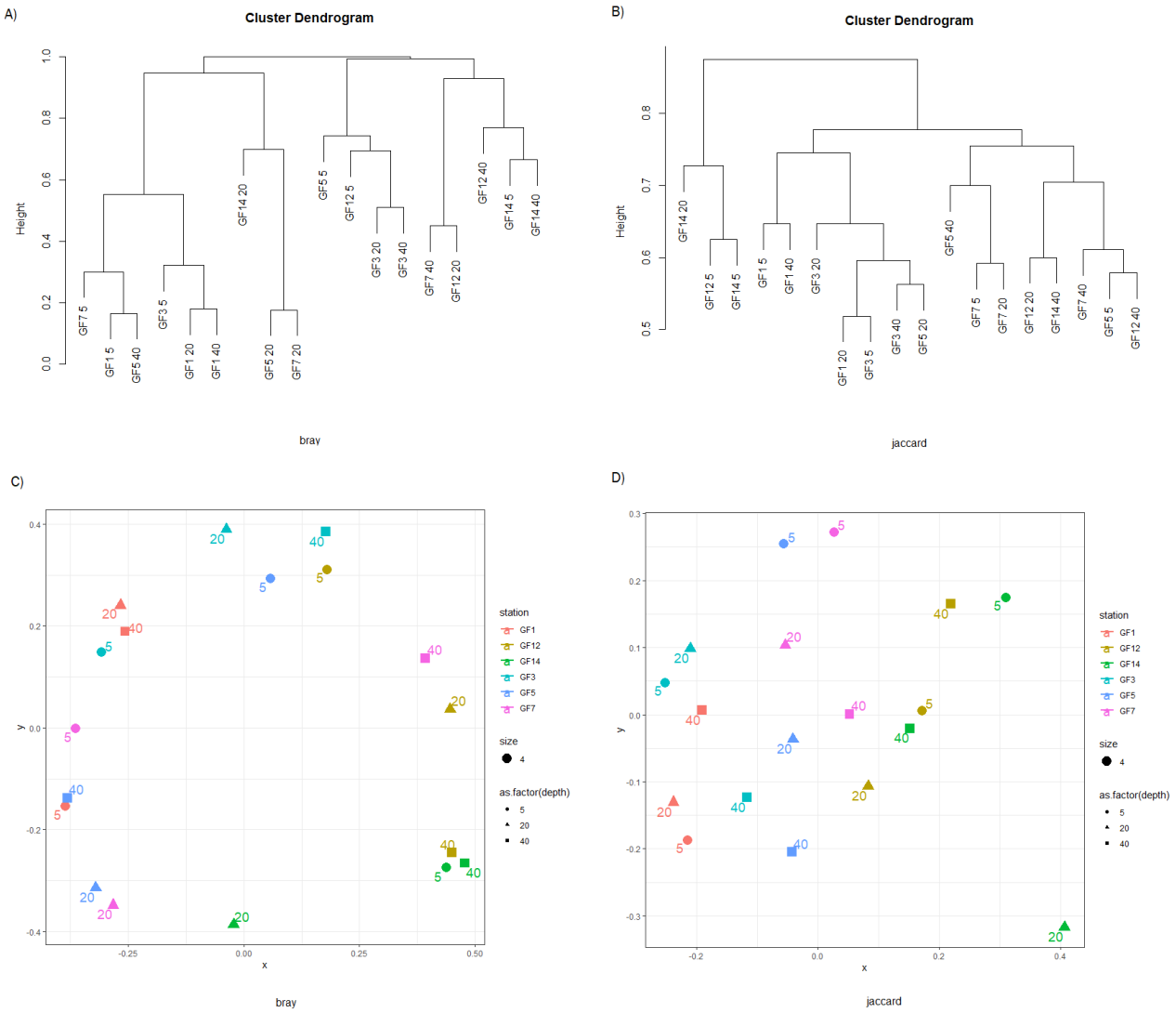

Figure 24 Hierarchic cluster dendrogram with A) Bray-Curtis and B) Jaccard dissimilarity (=height) and multidimensional scaling based on C) Bray-Curtis (stress = 0.050) and D) Jaccard (stress = 0.200) similarity index.

The hierarchical cluster analysis based on Jaccard dissimilarity index (Figure 24 B) revealed that all samples were grouped at ca. 50-80% axis height i.e. community composition between the samples was similar in 50-20%. Based on the Bray-Curtis similarity some of the samples shared > 80% of the species pool (Figure 24 A). For example, GF7 20 m and GF5 20 m had more than 80% similar species composition. The same occurred between GF1 5 m and GF5 40 and between GF1 20 m and GF1 40 m as well. Together these last two groups overlapped only little more than 40 %. Wide distribution of GF5 and GF7 was also seen from the hierarchal cluster analysis (Figure 24 C). Even though GF 5 20 m and GF7 20 m were grouped by the same depth and GF1 20 m and GF 40 m are from the same stations, in general samples did not cluster according to station and/or depth with hierarchical cluster analysis.

5.5 Primary productivity

Primary productivity was greater in the outer and middle stations than in the innermost stations although the highest integrated chl *a* and phytoplankton abundance were found at GF14 close to the glacier (Table 8). The station with lowest primary productivity, integrated chl *a* ratio and cell algal abundances was GF12. For example, the integrated chl *a* at GF12 was only 25% of the chl *a* value at GF14. Primary productivity was highest at GF1 followed by GF5 and GF7. At GF5 and GF7 there were also the second and third highest integrated cell counts and chl *a* values (Table 8). Calculated primary productivity per depth can be seen as an Appendix 2.

Table 8 Integrated primary productivity, chl *a*, phytoplankton abundance and depth of the photic zone for full stations.

Station	Primary productivity (mg C m^{-2} d^{-1} from 0 to 50 m)	Integrated chl *a* (mg m^{-2} from 0 to 50 m)	Integrated algal abundance (*10^9 cells m^{-2} from 0 to 50 m)	Depth of the photic zone (m)
GF1	1273	67.5	74.4	16
GF3	822	59.5	34.3	31
GF5	1153	69.4	147.0	17
GF7	1150	175	152.9	15
GF12	519	45.5	7.1	21
GF14	892	199	485.6	12

6. Discussion

The results show clear vertical and horizontal gradients of physical variables within the fjord system that modified phytoplankton community composition and primary production. In the following I will first discuss the physical features and their changes as related to the impact of glacial meltwater. This will be followed by a discussion of the relation between nutrients and phytoplankton species composition, abundance, biomass (chl *a*) and primary production. To conclude, I will discuss how climate change may alter physical features and nutrient flows in the Arctic fjord-system and how this affects Arctic phytoplankton and primary production.

6.1 Physical environment

The fjord stations showed strong temperature and salinity-based stratification excluding the outermost stations where water masses were more mixed. At station GF2, the surface water was stratified but after the first two meters the temperature and salinity gradients were relatively small compared to the middle and innermost stations. Similar to previous studies (Meire et al., 2015; Mortensen et al., 2018) this suggests that the surface waters at the outermost stations were highly affected by inflow of the coastal waters, whereas stations from

GF14 until GF8 were greatly affected by the glacial meltwater. Water temperatures above 3˚C at stations GF4 and GF5 at 50 m depth indicate that these layers were influenced by the warm coastal water whereas the upper water column was still affected by the glacial meltwater (Meire et al., 2015; Mortensen et al., 2018).

Surface water salinity differed greatly between the outer, middle and inner stations. In the IF fresh (salinity < 10) and cold surface water was highly influenced by glacial run-off. Salinity also highly stratified the upper water column, increasing rapidly from the surface until around 60 m depth. A similar pycnocline and strong gradient between 0 and60 m depth, efficiently preventing the mixing of water column, was also found in previous studies (Krawczyk et al., 2015). In the IF, the same kind of stratification between 7–10 m (the depth of summer surface layer) and more steady change of salinity until 50 m (the depth of subglacial discharge water) was also described in previous studies and related to increased meltwater runoff from glaciers (Juul-Pedersen et al., 2015; Mortensen et al., 2013, 2018). The mixing of these two water masses between GF4 and GF3 are seen from both the temperature and salinity plots (Figure 2 and 3) as also described in Mortensen et al. (2018).

When comparing the depth of cold water and salinity gradients, the salinity gradient around 31.5 defined the separation of fjord water affect by subglacial meltwater from the underlying coastal water (Mortensen et al., 2011). The water in the upper water column until 30–60 m maintained average phosphate concentrations but relatively high NOx concentrations in the fresh and especially in the cold-water columns near the glacier termini.

6.2 Light limitation

Light is a key factor for controlling algal growth in the marine ecosystems (Harrison et al., 1990; Leu et al., 2015). High light (PAR) surface irradiance from stations GF8 to GF1, excluding GF3, were due to sunny weather whereas sampling at the innermost stations were conducted on cloudy days. The average depth (17 m) of the photic zone was representative for most stations except in GF3 where the photic zone reached 31 m. This can be explained by the well mixed and clear water column at GF3 (Figure 2 and 3; Mortensen et al., 2018). The photic zone in GF12 was also surprisingly deep, most probably because of relatively low planktonic cells and organic particles concentrations, causing little light attenuation in the water column.

The shallowest depths for the photic zone were found in GF14 and GF11. Meltwater rivers can contain a lot of silica and are often more turbid than upwelling water being high in phosphate and nitrogen but low in silicate (Meire et al., 2016; Murray et al., 2015). Hence, turbid melt water might be the reason for shallow photic zone in GF11 and GF14 and also relatively high silicate concentration at station GF14 (Figure 4 and Figure 6).

6.3 Distribution of nutrients

Based on Principal Component Analysis, increasing distance from the glacier was correlated with changes in temperature and silicate concentrations. Also, there was a strong collinearity between depth and phosphate concentrations. While phosphate concentrations were low in the surface water especially in the inner and middle stations, NOx concentrations were lowest in the outer fjord and highest in the inner fjord (Figure 5 and 7). Silicate was found to be lowest around 20–30 m depth and below the detection limit in the whole water column at GF12 (Figure 6), which was the only station with the low abundance of *C. socialis* at every depth.

NOx concentrations were below the detection limit at the depth of 5 m in all stations except at GF3. Thus, inorganic nitrogen ion concentrations were extremely low in the surface water influenced by surface runoff as well as the coastal water. Deeper waters, influenced by subglacial discharge, contained high nitrogen concentrations especially near the glacier termini. All these three water masses are mixed at GF3 resulting in relatively high surface nitrogen concentration (Mortensen et al., 2018). NOx concentration patterns were following nitrogen concentrations measured in August 2013 (Meire et al., 2017).

Similar pattern was also evident for phosphate with the difference compared to NOx that coastal water contained relatively high concentrations of phosphate. While phosphate concentrations were low in the surface layer and high in the subglacial meltwater column, mixing at GF3 resulted in intermediate phosphate concentrations in the upper water column.

Furthermore, all of the nutrient measurements (excluding silicate concentration under the detection limit in the deeper water at station GF12) were similar to concentrations measured previously during August (Juul-Pedersen at al., 2015; Meire et al., 2017).

While NOx concentration can be explained by the pattern of subglacial discharge water and phosphate also to be linked with the coastal water (Mortensen et al., 2018), silicate concentration did not follow any of these patterns. Since GF12 is located near glacial discharge area, melting of clear icebergs could be the reason for the low silicate

concentrations. Melting of icebergs has been estimated to be more than a fifth of the total runoff in Godthåbsfjord (Meire et al., 2016; Van As et al., 2014) with silicate concentrations ranging from below the detection limit in clear ice samples up to 18 µM in debris-rich ice samples (Meire et al., 2016). In addition, high NOx and phosphate concentrations at GF14, but relatively low at GF12 at the depth of subglacial discharge water (i. e. 20–50 m depth), supports that nutrient upwelling due to subglacial discharge has been reduced at GF12 compared to GF14. On the other hand, even though NOx and phosphate concentrations were lower at GF12 than at GF14, they were relatively high comparing to silicate concentrations. Instead, low silicate concentrations appeared to be highly linked with low algal biomass (*in situ* fluorescence and chl *a* measurements) and primary productivity, even though highest cell counts were found in potentially silicate limited waters.

6.4 *In situ* fluorescence and chlorophyll *a*

In general, the extracted chlorophyll *a* concentrations were in good agreement with data measured with the Seapoint Chlorophyll *a* Fluorometer (Figure 12). The highest chl *a* values were found in the IF and the chl *a* maximum was located in the upper 10–20 m (Figure 10 and 11). Average extracted chl *a* concentrations in the upper 50 m ranged from 1.0 µg/l (GF12) to 3.6 µg/l (GF14). This is above the values from a previous study during the autumn bloom, when chl *a* concentrations in the upper 60 m ranged from 0.5 to 2.5 µg/l (Krawczyk et al., 2015).Yet, the extracted chl *a* values in the present study were not high compared to spring bloom values, when the average chl *a* values can reach up to 9.5 µg/l (Krawczyk et al., 2015). Nevertheless, the *in situ* measured chl *a* maxima at the inner stations (excluding GF13) and at the station GF8 ranged from 19 µg/l to 40µg/l. These relatively high concentrations (compared to 10–25 µg/l measured at chl *a* maxima along the fjord in August 2013 by Meire et al., 2017) suggest that the autumn bloom was peaking in the IF whereas in the OF the autumn bloom was still developing.

Fluorescence values above 3µg/l were found in the subsurface chlorophyll *a* maxima around 15 m depth at all the station except at GF3. In the Arctic subsurface chlorophyll maxima are common in stratified water columns when surface water has become exhausted from the nutrients and primary production is more efficient closer to higher nutrient concentrations at the bottom of photic zone (Brown et al., 2015; Martin et al., 2010; Tremblay et al., 2008). Because the water column was not stratified in GF3 due to mixing, also no clear subsurface chl *a* maximum occurred.

Generally, inorganic nutrient concentrations at the chl *a* maximum were low but increased progressively below the chl *a* maximum. This indicates that phytoplankton had already used most of the available nutrients at the current depth but may grow on nutrients coming to that specific depth from below, e.g. due to tidal mixing or diffusion across the thermo- and halocline (Brown et al., 2015; Merie et al., 2017).

6.5 Phytoplankton species composition

The results demonstrated a clear link between the environmental settings and the phytoplankton community composition. For example, low silicate values (≤ 2.0µM) and samples with silicate as a limiting nutrient (i.e. low N:Si ratio, Table 3) were usually related to high dominance (≥ 90%) of *Chaetoceros socialis* (Figure 15), which, like all diatoms, incorporates silicate into its frustule and hereby reduces dissolved silicate concentrations. It is crucial to remember that only diatoms and silicoflagellates are limited by silicate. Also, the Redfield ratio between nitrogen and silicate is only an average ratio and nutrient requirements of different species might vary greatly even inside the same phylogenic group (Tilman et al., 1982).

Low concentrations of NOx were usually related to relatively high presence (9–46%) of *Dinobryon balticum*, as observed at stations GF7 and GF5 at 5 m and station GF3 at every counted depth. *Dinobryon* genus is known to be mixotrophic and *D. balticum* colonies might utilize bacteria-rich microaggregates and fecal pellets in nutrient poor or light limited waters (McKenzie et al., 1995).

Clearly, stations with the highest algal biomass (chl *a*; Figure 10 and 11) and algal abundances (Figure 14) were dominated by *C. socialis* (Figure 15). At the same time, samples with low contributions of *C. socialis* (GF5, GF12 and GF14 5 m, and GF14 40 m) had the lowest total cell counts. Conclusively, primary productivity and phytoplankton species composition were strongly driven by this diatom species during autumn in Godthåbsfjord (Krawczyk et al., 2018).

The high contribution of *Chaetoceros socialis* with 92 % of the total abundance is contrary to observations from Krawczyk et al. (2015). However, a later study (Krawczyk et al., 2018) found *C. socialis* to be the dominant group during autumn, associated with fresher water conditions. In general, *Chaetoceros* species have been reported as an abundant species in many Arctic

regions (Booth & Horner, 1997; Degerlund & Eilertsen, 2010) and found most abundant at low salinities in an experimental study (≤ 12.2) (Zhang et al., 1999).

Chaetoceros socialis is listed by Guiry and Guiry (2020) as a harmful species but does not contain deleterious polyunsaturated aldehydes. It is insufficient food for some zooplankton species such as the copepod *Temora longicornis* (Koski et al., 2008) and might cause physical damage to fish gills (Sunesen et al., 2008). This indicates that *C. socialis* might experience a low grazing pressure and does not support upper trophic levels of the pelagic food web as efficiently as blooms dominated by some other phytoplankton species such as *Phaeocystis pouchetii* (Arendt et al., 2010).

However, results from the North Water Polynya suggest that *C. socialis* could be an important factor supporting such a biological richness of the region (Booth et al., 2002). In the North Water Polynya highest abundance of *C. socialis* was observed with 30 100 000 cell/l (Booth et al., 2002) which is close to abundances at GF14 20 m (27 738 890 cells/l). This highly productive polynya located in northern Baffin Bay is well-known of a rich ecosystem providing living areas for numerous high trophic marine mammals.

6.6 Similarity of species composition

The Shannon diversity index has previously been reported to be mostly under 2.0 in Godthåbsfjord (Krawczyk et al., 2018). In the present study the Shannon diversity varied greatly between samples from 0.03 (GF14 20 m) to 2.64 (GF14 40 m; Figure 18). However, the average diversity of all the stations was only 1.30, whereas in 2013 the highest diversity was reported to be 1.8 in September and the lowest 1.2 in May (Krawczyk et al., 2018).

Even though samples at GF1 and GF3 did not show specific clustering in hierarchal dendrogram, based on multidimensional scaling samples (especially 5 m and 20 m) resembled each other more than other samples taken from the same station. This pattern is most likely due to mixing water column at GF1 and GF3, which maintained the similar physical conditions and species composition between different depths.

The strong dominance of a single species (C*. Socialis)* also explains the similarity of samples seen in the hierarchical cluster dendrogram based on Bray-Curtis index but not with Jaccard. While Jaccard index takes into consideration only presence or absence of a certain species, Bray-Curtis index considers species relative abundances and thus does not overestimate the

impact of rare species with low magnitudes that occurred in all samples (excluding GF14 20 m).

Strong positive correlation between total cell counts and chl *a* supports the accuracy of cell counts. While Pielou's evenness index and chl *a* concentrations were negatively correlated, species richness and chl *a* concentrations were positively correlated. This confirms previous findings that communities with higher number of species produce more biomass (Cardinale et al., 2011), but a negative relationship between evenness and primary production is often observed, when communities are strongly dominated by one highly productive species like in this study (Lewandowska et al., 2016).

Based on linear regression model between extracted PCA Dimension 1 and chl *a*, the later increased while Dimension 1 (mainly driven by NOx but also by phosphate salinity and depth) decreased. High nutrient fixation by phytoplankton is required to maintain high biomass and chl *a* concentrations, resulting in low nutrient and especially low NOx levels (Tremblay & Gagnon, 2009).

Also, relationship between species richness and Dimension 2 (mainly driven by temperature but also distance and silicate) was negative. In other words, closer to the glaciers (where the water temperature and distance to glacier were lower) there were more species but lower species richness. This together with the negative relationship between total cell counts and Pielou's evenness supports a theory by Lewandowska et al. (2016) suggesting that high productivity is maintained by dominant species i. e. in this study *Chaetoceros socialis*.

6.7 Primary productivity

In general, measured primary productivity was relatively high (compared to Meire et al., 2017) but not unprecedented (Juul-Pedersen et al., 2015). In this study average primary productivity at all stations was 968.2 mg C m^{-2} d^{-1} whereas in August 2013 the highest measured primary productivity was only 550 mg C m^{-2} d^{-1} (Meire et al., 2017) and in July 2010 the measured average primary productivity at station GF3 was 1382.5 mg C m^{-2} d^{-1} (Juul-Pedersen et al., 2015).

As describes for chl *a* maxima, in the inner fjord primary productivity maxima (Appendix 2) coincided with potential silicate limitation. At the middle station, maximum was in between the NOx limitation at 10 m depth and Si limitation at 20 m depth (Table 3). Also, when comparing silicate concentrations (Figure 7) and primary productivity (Appendix 2) low silicate

concentration at GF12 was accompanied with low primary productivity, and at GF14 two primary productivity peaks collided with lower silicate concentrations.

The highest integrated primary productivity was measured at GF1, while the whole water column was potentially nitrogen limited (Table 3). Integrated algal abundance and biomass (chl *a*) were relatively high, and in addition species richness was one of the highest while the station was strongly dominated by *C. socialis*.

The highest integrated cell counts were discovered at station GF14 alongside with the highest integrated chl *a* values. However, based on primary productivity analysis GF14 was one of the most unproductive stations. Inorganic nitrogen analysis revealed, that even though at GF14 there was high NOx concentrations below 20 m, concentrations were low in the surface layer. In fact, cell counts at sample GF14 5 m were the second lowest, right after station GF14 40 m. This suggests that surface waters were already depleted from nitrogen, as shown by the nutrient data (Figure 7 and Table 3). Based on fluorescence CTD measurements exceptionally high chl *a* maximum was located at the depth of 11 m, which was just above the aphotic zone, but productive phytoplankton could still receive nitrogen from below the photic zone (12 m; Brown et al., 2015).

While high cell counts, average primary productivity and high concentrations of chl *a* as well as silicate were observed at station GF14, the lowest cell counts, primary productivity, silicate and chl *a* concentrations were found at station GF12. In addition to previously mentioned explanations related to meltwater of clear icebergs and reduced effects of nutrient upwelling, one reason for exceptionally low silicate concentrations at GF12 might be uptake by an already peaked diatom dominated autumn bloom which could have depleted silicate before sinking to the bottom (i. e. autumn bloom maxima would first occur at GF12 before GF14). This is supported by the low silicate concentrations which collided together with high productivity whereas the physical explanations are supported by the low concentration found not only in the upper water column but also down to 100 m depth. In this case low silicate concentration had prevented phytoplankton community to bloom at this station. On the other hand, if the low silicate concentrations had been long-term condition, it is likely that the community would have been dominated by non-silicate required species. The sample GF12 20 m was clearly *C. socialis* dominated although the phytoplankton abundance was very low.

6.8 Future predictions

The mass balance of Greenland ice sheet switched from gaining ice in 1972–1980 to loosing mass every decade since 1980 (Mouginot et al., 2019). On average, in 2010–2018 the mass loss of Greenland Ice sheet was six times higher (286 ± 20 Gt/y) as it was in 1980–1990 (51 ± 17 Gt/y) (Mouginot et al., 2019). In addition, Greenland Ice sheet is documented to slide on top of the bedrock to calving front regions and especially fast in the western coastal regions, which will increase the carving of glacier fronts (Maier et al., 2019).

Increased carving process will increase nutrient upwelling in marine-terminating glacier-fjord systems. This will increase primary production and might alter phytoplankton community composition to strong dominance by one or few species, which might not be as effective in transferring energy to upper trophic levels in the marine food web.

Based on recent studies, Greenland Ice sheet will gain mass only one year in a century and will lose mass the remaining 99 years (King et al., 2020). Thus, it is likely that the Greenland Ice sheet will continue to melt, at least until the marine terminating glaciers will shift to land terminating glaciers. Upwelling due to calving fronts and meltwater buoyance will be lost and freshening of surface water due to meltwater rivers might lead the stratification to be more persistent preventing wind-driven upwelling (Tremblay & Gagnon, 2009). In this case primary production will decrease and might not be adequate to maintain the rich Arctic biota. Thus, a shift to new Arctic marine ecosystems is expected.

7. Limitations of the study

As always in the science, there is room for human errors, and in this study those errors are more plausible to occur with species identification than with any other work phase. Some of the species were easier to identify than others, making it possible to have a biased data. Also, some of the samples contained a huge amount of cells, where not counting one cell is not impacting the final result as in samples containing only few cells. Some of the samples were almost empty making an individual cell representing a larger share of the phytoplankton community in that sample. Also, some of the samples were clearer than others making it easier to identify cells to species level, whereas some of the species — especially in darker samples — were impossible to identify to species level with inverted light microscope.

All measurements taken at sea or analyses made in the lab contain intrinsic errors. *In situ* fluorescence data in the immediate vicinity of the surface might be biased since the CTD

fluorometer can be saturated by surrounding light. When calculating photic zone from the irradiance data, the 1 m depth value was used as a surface value as it was challenging to take an exact reading when the sensor breaks the surface on a moving vessel. Calculating the 1% PAR value using the 1 m instead of a true surface value leads to a slight overestimation of the depth of the euphotic zone.

Temporal limitation of the study is obvious since all the sampling and measurements were done only once. It would be interesting to repeat the sampling over a longer time period to know if the maximum of the bloom had already been achieved or if the bloom was still developing. However, this study focused on the spatial gradients in physical and chemical variables and the related biological patterns, while time constraints and the single sampling of each station did not allow for a temporal perspective.

The total length of the transect also imposed limitations to the number of stations, thus resulting in a significant difference in distance between stations, especially between GF8 and GF11. Ideally more stations could have been added also after GF1 towards to the open ocean and between GF14 and the end of the fjord, to get wider understanding of the fjord transect.

The vertical resolution of the measurements is limited by the available time in the field as well as time for laboratory analysis of samples. The fluorescence maximum was often located between the discrete sampling depths (e.g. between 10 m and 20 m), thus maximum values may have been missed during sampling for nutrients, extracted chl a and for cell counts. This may have led to missing the deep chl *a* maximum and potentially underestimating the integrated chl *a* and algal abundances. Species composition and abundances only represents 5 m, 20 m and 40 m, thus potentially missing dense phytoplankton cell concentrations. Also, primary productivity was calculated only from samples taken from 5 m and 20 m depths, which potentially increases the error of estimates based on P-I curve incubations. Also, possible errors with surface *in situ* fluorescence data would impact the to primary production calculation but only slightly since primary production in the upper 1 m was always close to zero.

8 Conclusion

The hydrography in the fjord was highly impacted by the freshwater run-off coming from the glacier. Stations in the IF were less saline and there existed a cold sub-surface water lens indicating that stratification in the upper ca. 10 m was mainly caused by surface runoff, and the water column from 10 m to 30–50 m was mainly affected by subglacial discharge. This upper

water column also contained more dissolved inorganic nitrogen, which sustained high phytoplankton abundance in the water column, which was not limited by light or silicate. The outermost stations were mainly affected by coastal water containing low nitrogen, but relatively high phosphate concentrations.

Moreover, in contrast to Tremblay and Gagnon (2009) stating nitrogen as the limiting nutrients in the Arctic systems, the present study suggests silicate as the limiting nutrient within the photic zone in the inner part of the fjord in autumn. Increasing silicate input from glaciers (Meire et al., 2016) could positively alter primary production. Nevertheless, also nitrogen input would most likely accelerate primary productivity especially in the OF regions.

Chlorophyll *a* concentrations and cell counts were higher in the IF than OF indicating that autumn bloom was peaking in the IF. However, phytoplankton was concentrated in thinner layers in the water column of the IF, which resulted in higher integrated primary productivity in the OF. Subglacial upwelling had clear positive influence on phytoplankton growth and primary productivity. Surface meltwater contributed silicate but also reduces light penetration lowering total primary productivity. This might have caused primary productivity to be higher in the OF than IF.

Nutrient concentrations were determined by the physical factors of the fjord, which regulated phytoplankton abundance and biomass (chl *a*). Thus, it is fair to say that glacial meltwater and/or subglacial discharge contributed higher phytoplankton abundance and chl *a* concentrations, whereas primary productivity was also dependent on other features such as vertical mixing and light availability.

The possible nitrogen limitation was often associated with dominance of mixotrophic *Dinobryon balticum* while low silicate concentrations were linked to high cell counts and dominance of *Chaetoceros socialis*. Most of the stations were highly dominated by *C. socialis*, which determined total phytoplankton community abundance and primary productivity. High dominance (i. e. low Pielou's evenness index) was also related to high species richness.

Even though *C. socialis* and *D. balticum* occurrences were linked to nutrient concentrations, species composition analysis based on Bray-Curtis did not reveal clear pattern and based on Jaccard index was difficult to interpret. Thus, it was concluded that species composition was randomly distributed and not influenced by glacial meltwater. However, it might be possible that due to the highly dominant *C. socialis,* interactions for other taxa were hidden. Thus, it would be valuable to repeat such study between the spring and autumn bloom, when

phytoplankton community might be more evenly distributed. Also, this study included only selected species smaller than 5 µm and bacterioplankton was not examined at all. These small size plankton taxa are predicted to become more abundant in the Arctic water (Li et al., 2009) and need to be studied more closely and included more diligently in future studies.

Addressing the initially posted 2 hypotheses, it can be stated: that 1) biomass (chlorophyll *a*) and phytoplankton abundance were higher in the IF than the OF stations while primary productivity was higher in the OF. Also, closer to the glacier there was a higher number of species and more dominated community composition than in the OF stations.

It is clear, that physical features of marine terminated fjord define the primary productivity, phytoplankton abundance and species composition it this Arctic fjord. Thus, global warming and retrieving of glaciers will affect the whole ecosystem of this fjord and consequently change the productivity of the fjord. When melting of ice accelerates, the upwelling effect might increase leading to transitory increase of primary production. At the same time increased runoff from land terminating glaciers might increase silicate concentrations benefiting diatom species, although turbid runoff water will also decrease the depth of photic zone resulting in decrease of primary productivity. Nevertheless, if marine-terminating glaciers retreat further and become land-terminating glacier, primary productivity will eventually decrease, since the lack of nutrient upwelling will lead to fast exhaustion of nitrogen in stratified water column produced by meltwater rivers.

Acknowledgement

This study was carried out together with Greenland Climate Research Centre (GCRC), UiT The Arctic University of Norway and Helsinki University. The study was conducted in collaboration with Greenland Ecosystem Monitoring (GEM), MarineBasis-Nuuk monitoring program. I am extremely thankful for all the boat time, equipment and laboratory space GCRC offered me. Also, I am very grateful of being able to cover travel costs to Greenland with the grant I had received from Maaperä- ja vesitekniikan tuki ry.

Especially I want to thank all my supervisors: Thomas for making this project possible, Rolf for believing in my developing species identification skills and Aleksandra for building up my self-confidence and understanding about statistics. It has been truly an amazing experience to have not one but three so ambitious and encouraging supervisors. I could not make this happen without your continuous help, and there was much I learned form you that goes beyond my thesis.

I would like to thank Else Ostermann and Michael Kristiansen for priceless lab assistance and hard work in the field. I would like to thank Fleming Heinrich for sailing us safe and sound back and forth the Godhåbsfjord and Lorenz Meire who repeatedly was helping me with R programming language.

In the end I would like to thank my family and especially my mother who believed I would do better as a marine biologist than a confectioner.

References

Arendt, K. E., Nielsen, T. G., Rysgaard, S., & Tönnesson, K. (2010). Differences in plankton community structure along the Godthåbsfjord, from the Greenland Ice Sheet to offshore waters. *Marine Ecology Progress Series*, *401*, 49-62. https://doi.org/10.3354/meps08368

Bendtsen, J., Mortensen, J., Lennert, K., & Rysgaard, S. (2015). Heat sources for glacial ice melt in a west Greenland tidewater outlet glacier fjord: The role of subglacial freshwater discharge. *Geophysical Research Letters*, *42*(10), 4089-4095. https://doi.org/10.1002/2015GL063846

Booth, B. C., & Horner, R. A. (1997). Microalgae on the Arctic Ocean Section, 1994: species abundance and biomass. *Deep Sea Research Part II: Topical Studies in Oceanography*, *44*(8), 1607-1622. https://doi.org/10.1016/S0967-0645(97)00057-X

Booth, B. C., Larouche, P., Bélanger, S., Klein, B., Amiel, D., & Mei, Z. P. (2002). Dynamics of Chaetoceros socialis blooms in the North Water. *Deep Sea Research Part II: Topical Studies in Oceanography*, *49*(22-23), 5003-5025. https://doi.org/10.1016/S0967-0645(02)00175-3

Bray, J. R., & Curtis, J. T. (1957). An ordination of the upland forest communities of southern Wisconsin. *Ecological monographs*, *27*(4), 325-349. https://doi.org/10.2307/1942268

Brown, Z. W., Lowry, K. E., Palmer, M. A., van Dijken, G. L., Mills, M. M., Pickart, R. S., & Arrigo, K. R. (2015). Characterizing the subsurface chlorophyll *a* maximum in the Chukchi Sea and Canada Basin. *Deep Sea Research Part II: Topical Studies in Oceanography*, *118*, 88-104. https://doi.org/10.1016/j.dsr2.2015.02.010

Brzezinski, M. A. (1985). The Si:C:N ratio of marine diatoms: Interspecific variability and the effect of some environmental variables 1. *Journal of Phycology*, *21*(3), 347-357. https://doi.org/10.1111/j.0022-3646.1985.00347.x

Calbet, A., Riisgaard, K., Saiz, E., Zamora, S., Stedmon, C., & Nielsen, T. G. (2011). Phytoplankton growth and microzooplankton grazing along a sub-Arctic fjord (Godthåbsfjord, west Greenland). *Marine Ecology Progress Series*, *442*, 11-22. https://doi.org/10.3354/meps09343

Cardinale, B. J., Matulich, K. L., Hooper, D. U., Byrnes, J. E., Duffy, E., Gamfeldt, L., ... & Gonzalez, A. (2011). The functional role of producer diversity in ecosystems. *American journal of botany*, *98*(3), 572-592. https://doi.org/10.3732/ajb.1000364

Chase, J. M., & Knight, T. M. (2013). Scale-dependent effect sizes of ecological drivers on biodiversity: why standardised sampling is not enough. *Ecology letters*, *16*(s1), 17-26. https://doi.org/10.1111/ele.12112

Cheng, J., Karambelkar, B., & Xie, Y. (2018). *Leaflet: Create interactive web maps with the JavaScript 'leaflet' library*. R package version 2.0.2. https://CRAN.R-project.org/package=leaflet.

Degerlund, M., & Eilertsen, H. C. (2010). Main species characteristics of phytoplankton spring blooms in NE Atlantic and Arctic waters (68–80 N). *Estuaries and coasts*, *33*(2), 242-269. https://doi.org/10.1007/s12237-009-9167-7

García-Robledo, E., Corzo, A., & Papaspyrou, S. (2014). A fast and direct spectrophotometric method for the sequential determination of nitrate and nitrite at low concentrations in small volumes. *Marine Chemistry*, *162*, 30-36. https://doi.org/10.1016/j.marchem.2014.03.002

Grasshoff, K, Erhardt, M & Kremling, K. (1983). *Methods of seawater analysis*. (2nd edition). Verlag Chemie. Weinheim.

Guiry, M.D. & Guiry, G.M. (2020). *AlgaeBase*. World-wide electronic publication, National University of Ireland, Galway. https://www.algaebase.org.

Harrison, P. J., Thompson, P. A., & Calderwood, G. S. (1990). Effects of nutrient and light limitation on the biochemical composition of phytoplankton. *Journal of Applied Phycology*, *2*(1), 45-56. https://doi.org/10.1007/BF02179768

HELCOM. (2017). *Monitoring of phytoplankton species composition, abundance and biomass.* https://helcom.fi/wp-content/uploads/2019/08/Guidelines-for-monitoring-phytoplankton-species-composition-abundance-and-biomass.pdf

Hotelling, H. (1933). Analysis of a complex of statistical variables into principal components. *Journal of educational psychology*, *24*(6), 417-441 & 489-520. https://doi.org/10.1037/h0071325

Jaccard, P. (1912). The distribution of the flora in the alpine zone. 1. *New phytologist*, *11*(2), 37-50. https://doi.org/10.1111/j.1469-8137.1912.tb05611.x

Juul-Pedersen, T., Arendt, K. E., Mortensen, J., Blicher, M. E., Søgaard, D. H., & Rysgaard, S. (2015). Seasonal and interannual phytoplankton production in a sub-Arctic tidewater outlet glacier fjord, SW Greenland. *Marine Ecology Progress Series*, *524*, 27-38. https://doi.org/10.3354/meps11174

Karlson, B., Andreasson, A., Johansen, M., Karlberg, M., Loo, A., Skjevik, A-T. (2018). *Nordic Microalgae*. World-wide electronic publication, http://nordicmicroalgae.org.

Kassambara, A., & Mundt, F. (2020). *factoextra: Extract and visualize the results of multivariate data analyses*. R package version 1.0.7. https://CRAN.R-project.org/package=factoextra.

King, M. D., Howat, I. M., Candela, S. G., Noh, M. J., Jeong, S., Noël, B. P., ... & Negrete, A. (2020). Dynamic ice loss from the Greenland Ice Sheet driven by sustained glacier retreat. *Communications Earth & Environment*, *1*(1), 1-7. https://doi.org/10.1038/s43247-020-00019-0

Koski, M., Wichard, T., & Jónasdóttir, S. H. (2008). “Good” and “bad” diatoms: development, growth and juvenile mortality of the copepod *Temora longicornis* on diatom diets. *Marine Biology*, *154*(4), 719-734. https://doi.org/10.1007/s00227-008-0965-4

Krawczyk, D. W., Witkowski, A., Juul-Pedersen, T., Arendt, K. E., Mortensen, J., & Rysgaard, S. (2015). Microplankton succession in a SW Greenland tidewater glacial fjord influenced by coastal inflows and run-off from the Greenland Ice Sheet. *Polar Biology*, *38*(9), 1515-1533. https://doi.org/10.1007/s00300-015-1715-y

Krawczyk, D. W., Meire, L., Lopes, C., Juul-Pedersen, T., Mortensen, J., Li, C. L., & Krogh, T. (2018). Seasonal succession, distribution, and diversity of planktonic protists in relation to hydrography of the Godthåbsfjord system (SW Greenland). *Polar Biology*, *41*(10), 2033-2052. https://doi.org/10.1007/s00300-018-2343-0

Leu, E., Mundy, C. J., Assmy, P., Campbell, K., Gabrielsen, T. M., Gosselin, M., ... & Gradinger, R. (2015). Arctic spring awakening–Steering principles behind the phenology of vernal ice algal blooms. *Progress in Oceanography*, *139*, 151-170. https://doi.org/10.1016/j.pocean.2015.07.012

Lewandowska, A. M., Biermann, A., Borer, E. T., Cebrián-Piqueras, M. A., Declerck, S. A., De Meester, L., ... & Harpole, W. S. (2016). The influence of balanced and imbalanced resource supply on biodiversity–functioning relationship across ecosystems. *Philosophical Transactions of the Royal Society B: Biological Sciences*, *371*(1694), 20150283. https://doi.org/10.1098/rstb.2015.0283

Li, W. K., McLaughlin, F. A., Lovejoy, C., & Carmack, E. C. (2009). Smallest algae thrive as the Arctic Ocean freshens. *Science*, *326*(5952), 539. https://doi.org/10.1126/science.1179798

Maier, N., Humphrey, N., Harper, J., & Meierbachtol, T. (2019). Sliding dominates slow-flowing margin regions, Greenland Ice Sheet. *Science advances*, *5*(7), 1-10. https://doi.org/10.1126/sciadv.aaw5406

Martin, J., Tremblay, J. É., Gagnon, J., Tremblay, G., Lapoussière, A., Jose, C., ... & Michel, C. (2010). Prevalence, structure and properties of subsurface chlorophyll maxima in Canadian Arctic waters. *Marine Ecology Progress Series*, *412*, 69-84. https://doi.org/10.3354/meps08666

McKenzie, C. H., Deibel, D., Paranjape, M. A., & Thompson, R. J. (1995). The marine mixotroph Dinobryon balticum (Chrysophyceae): Phagotrophy and survival in a cold ocean[1]. *Journal of Phycology*, *31*(1), 19-24. https://doi.org/10.1111/j.0022-3646.1995.00019.x

Meire, L., Søgaard, D. H., Mortensen, J., Meysman, F. J. R., Soetaert, K., Arendt, K. E., ... & Rysgaard, S. (2015). Glacial meltwater and primary production are drivers of strong CO2 uptake in fjord and coastal waters adjacent to the Greenland Ice Sheet. *Biogeosciences*, *12*(8), 2347-2363. https://doi.org/10.5194/bg-12-2347-2015

Meire, L., Meire, P., Struyf, E., Krawczyk, D. W., Arendt, K. E., Yde, J. C., ... & Meysman, F. J. R. (2016). High export of dissolved silica from the Greenland Ice Sheet. *Geophysical Research Letters*, *43*(17), 9173-9182. https://doi.org/10.1002/2016GL070191

Meire, L., Mortensen, J., Meire, P., Juul-Pedersen, T., Sejr, M. K., Rysgaard, S., ... & Meysman, F. J. (2017). Marine-terminating glaciers sustain high productivity in Greenland fjords. *Global Change Biology*, *23*(12), 5344-5357. https://doi.org/10.1111/gcb.13801

Meunier, A. (1910). *Microplankton des Mers de Barents et de Kara* (Vol. 1). C. Bulena.

Mortensen, J., Lennert, K., Bendtsen, J., & Rysgaard, S. (2011). Heat sources for glacial melt in a sub-Arctic fjord (Godthåbsfjord) in contact with the Greenland Ice Sheet. *Journal of Geophysical Research: Oceans*, *116*(C1). https://doi.org/10.1029/2010JC006528

Mortensen, J., Bendtsen, J., Motyka, R. J., Lennert, K., Truffer, M., Fahnestock, M., & Rysgaard, S. (2013). On the seasonal freshwater stratification in the proximity of fast-flowing tidewater outlet glaciers in a sub-Arctic sill fjord. *Journal of Geophysical Research: Oceans*, *118*(3), 1382-1395. https://doi.org/10.1002/jgrc.20134

Mortensen, J., Rysgaard, S., Arendt, K. E., Juul-Pedersen, T., Søgaard, D. H., Bendtsen, J., & Meire, L. (2018). Local coastal water masses control heat levels in a West Greenland tidewater outlet glacier fjord. *Journal of Geophysical Research: Oceans*, *123*(11), 8068-8083. https://doi.org/10.1029/2018JC014549

Mouginot, J., Rignot, E., Bjørk, A. A., Van Den Broeke, M., Millan, R., Morlighem, M., ... & Wood, M. (2019). Forty-six years of Greenland Ice Sheet mass balance from 1972 to 2018. *Proceedings of the National Academy of Sciences*, *116*(19), 9239-9244. https://doi.org/10.1073/pnas.1904242116

Murray, C., Markager, S., Stedmon, C. A., Juul-Pedersen, T., Sejr, M. K., & Bruhn, A. (2015). The influence of glacial melt water on bio-optical properties in two contrasting Greenlandic fjords. *Estuarine, Coastal and Shelf Science*, *163*, 72-83. https://doi.org/10.1016/j.ecss.2015.05.041

Murtagh, F. (1985). *Multidimensional Clustering Algorithms*. Physica-Verlag, Vienna

Oksanen, J., Blanchet, F. G., Friendly, M., Kindt, R., Legendre, P., McGlinn, D., ... Wagner, H. (2019). *Vegan: Community ecology package*. R package version 2.5-6. https://CRAN.R-project.org/package=vegan.

Pielou, E. C. (1966). The measurement of diversity in different types of biological collections. *Journal of Theoretical Biology*, *13*, 131-144. https://doi.org/10.1016/0022-5193(66)90013-0

Platt, T., & Sathyendranath, S. (1995). *Software for Use in Calculation of Primary Production in the Oceanic Water Column*. http://www.ioccg.org/software/Ocean_Production/rpt.pdf.

R Core Team (2018). *R: A language and environment for statistical computing*. R Foundation for Statistical Computing, Vienna, Austria. https://www.R-project.org/.

Rao, C. R. (1964). The use and interpretation of principal component analysis in applied research. *Sankhyā: The Indian Journal of Statistics, Series A (1961-2002)*, *26*(4), 329-358. https://www.jstor.org/stable/25049339

Redfield, A. C. (1934). On the proportions of organic derivatives in sea water and their relation to the composition of plankton. *James Johnstone memorial volume*, 176-192.

Redfield, A. C. (1958). The biological control of chemical factors in the environment. *American scientist*, *46*(3), 230A & 205-221. https://www.jstor.org/stable/27827150

Rysgaard, S., Vang, T., Stjernholm, M., Rasmussen, B., Windelin, A., & Kiilsholm, S. (2003). Physical conditions, carbon transport, and climate change impacts in a northeast Greenland fjord. Arctic, Antarctic, and Alpine Research, *35*(3), 301-312. https://doi.org/10.1657/1523-0430(2003)035[0301:PCCTAC]2.0.CO;2

Schlitzer, R. (2020). Ocean Data View. https://odv.awi.de.

Shannon, C. E. (1948). A mathematical theory of communication. *The Bell system technical journal*, *27*(3), 379-423. https://doi.org/10.1002/j.1538-7305.1948.tb01338.x

Silsbe, G. M., & Malkin, S. Y. (2015). *Phytotools: Phytoplankton Production Tools*. R package version 1.0. https://CRAN.R-project.org/package=phytotools.

Slater, D. A., Straneo, F., Felikson, D., Little, C. M., Goelzer, H., Fettweis, X., & Holte, J. (2019). Estimating Greenland tidewater glacier retreat driven by submarine melting. *Cryosphere*, *13*(9), 2489-2509. https://doi.org/10.5194/tc-13-2489-2019

Steeman Nielsen, E. (1952). The use or radiocarbon (C^{14}) for measuring organic production in the sea. *ICES Journal of Marine Science J. Cons. Int. Explor. Mer*, *18*(2), 177-180. https://doi.org/10.1093/icesjms/18.2.117

Straneo, F., & Heimbach, P. (2013). North Atlantic warming and the retreat of Greenland's outlet glaciers. *Nature*, *504*(7478), 36-43. https://doi.org/10.1038/nature12854

Strickland, J.D.H. & Parsons, T.R. (1972). *A Practical Handbook of Seawater Analysis* (2nd edition). Bulletin 167, Fisheries Research Board of Canada, Ottawa, ON.

Sunesen, I., Hernández Becerril, D. U., & Sar, E. A. (2008). Marine diatoms from Buenos Aires coastal waters (Argentina). V. Species of the genus *Chaetoceros*. *Revista de Biología Marina y Oceanografía*, *43*(2), 303-326. https://doi.org/10.4067/S0718-19572008000200009

Sverdrup, H. U. (1953). On conditions for the vernal blooming of phytoplankton. *Journal du Conseil International pour l'Exploration de la Mer*, *18*(3), 287-295.

Syvitski, J. P., Burrell, D. C., & Skei, J. M. (1987). *Fjords: processes and products*. Springer Verlag, New York, NY

Throndsen, J., Hasle, G. R., & Tangen, K. (2007). *Phytoplankton of Norwegian coastal waters*. Almater Forlag AS.

Tilman, D., Kilham, S. S., & Kilham, P. (1982). Phytoplankton community ecology: The role of limiting nutrients. *Annual review of Ecology and Systematics*, *13*(1), 349-372. https://doi.org/10.1146/annurev.es.13.110182.002025

Tomas, C. R. (Ed.). (1997). *Identifying marine phytoplankton*. Elsevier.

Tremblay, J. É., Simpson, K., Martin, J., Miller, L., Gratton, Y., Barber, D., & Price, N. M. (2008). Vertical stability and the annual dynamics of nutrients and chlorophyll fluorescence in the coastal, southeast Beaufort Sea. *Journal of Geophysical Research: Oceans*, *113*, C07S90. https://doi.org/10.1029/2007JC004547

Tremblay, J. É., & Gagnon, J. (2009). The effects of irradiance and nutrient supply on the productivity of Arctic waters: a perspective on climate change. In: Nihoul J.C.J., Kostianoy A.G. (Eds.), *Influence of climate change on the changing arctic and sub-arctic conditions* (pp. 73-93). Springer, Dordrecht. doi:10.1007/978-1-402009460-6_7.

Utermöhl, H. (1958). Zur vervollkommnung der quantitativen phytoplankton-methodik. *Mitteilungen der Internationale Vereinigung für theoretische und angewandte. Limnologie*, *9*(1), 1-38.

Van As, D., Andersen, M. L., Petersen, D., Fettweis, X., Van Angelen, J. H., Lenaerts, J. T., ... & Steffen, K. (2014). Increasing meltwater discharge from the Nuuk region of the Greenland ice sheet and implications for mass balance (1960–2012). *Journal of Glaciology*, *60*(220), 314-322. https://doi.org/10.3189/2014JoG13J065

Webb, W. L., Newton, M., & Starr, D. (1974). Carbon dioxide exchange of *Alnus rubra*: A mathematical model. *Oecologia*, *17*(4), 281-291.

Wickham, H. (2016). *Ggplot2: Elegant graphics for data analysis* (2nd Edition). Springer-Verlag New York.

Zhang, Q., Gradinger, R., & Spindler, M. (1999). Experimental study on the effect of salinity on growth rates of Arctic-sea-ice algae from the Greenland Sea. *Boreal environment research*, *4*, 1-8.

Appendix 1: Complete list of identified phytoplankton species and cell counts (cells/l) per station (classified after Guiry & Guiry, 2020)

	Station	GF1	GF1	GF1	GF3	GF3	GF3	GF5	GF5	GF5	GF7	GF7	GF7	GF12	GF12	GF12	GF14	GF14	GF14
	Depth (m)	5	20	40	5	20	40	5	20	40	5	20	40	5	20	40	5	20	40
Group	Species																		
Bacillariophyceae	*Attheya septentrionalis* (Østrup) R.M.Crawford, 1994	15360	2941	5408	9013	6667	2500	4802	5661	3333	6667	10240	160	0	40	0	0	0	0
Bacillariophyceae	*Bacterosira bathyomphala* (Cleve) Syvertsen & Hasle, 1993	160	1828	0	2294	273	136	0	1890	1878	977	2056	0	0	480	100	0	0	0
Bacillariophyceae	*Bacteriosira* sp.	0	406	0	0	0	0	0	0	0	0	0	160	0	0	0	0	0	0
Bacillariophyceae	*Cerataulina pelagica* (P.T. Cleve) Hendey, 1937	0	0	0	0	137	0	134	0	0	0	0	80	0	0	20	0	0	0
Bacillariophyceae	*Chaetoceros affinis* Lauder, 1864	0	0	0	0	478	0	0	0	0	0	0	0	0	0	0	0	0	0
Bacillariophyceae	*Chaetoceros* cf *atlanticus* P.T. Cleve, 1873	0	0	0	0	0	0	0	0	0	0	294	0	0	0	0	0	0	0
Bacillariophyceae	*Chaetoceros borealis* J.W. Bailey, 1854	720	0	0	0	0	0	0	0	0	0	0	0	0	0	0	0	0	0
Bacillariophyceae	*Chaetoceros* cf *brevis* Schütt, 1895	0	0	0	0	0	0	0	0	0	0	56320	0	0	0	0	0	0	0
Bacillariophyceae	*Chaetoceros constrictus* Gran, 1897	0	0	0	0	0	0	0	0	1174	0	0	0	0	0	0	0	0	0
Bacillariophyceae	*Chaetoceros* cf *constrictus* Gran, 1897	0	0	40560	0	0	0	0	0	0	0	35840	0	0	0	0	0	0	0
Bacillariophyceae	*Chaetoceros contortus* Schütt, 1895	0	0	0	0	0	5407	0	0	0	0	1763	0	0	0	0	0	0	0
Bacillariophyceae	*Chaetoceros convolutus* Castracane, 1886	0	0	215	0	10000	0	0	0	0	0	0	400	0	0	0	0	0	0
Bacillariophyceae	*Chaetoceros* cf *costatus* Pavillard, 1911	0	0	0	0	546	0	0	0	0	0	441	0	0	0	0	0	0	0
Bacillariophyceae	*Chaetoceros curvisetus* P.T. Cleve, 1889	0	0	0	0	0	0	0	0	0	0	30720	0	0	0	0	0	0	0
Bacillariophyceae	*Chaetoceros* cf *curvisetus* P.T. Cleve, 1889	0	1523	0	3790	0	3118	134	0	2817	0	0	640	0	0	0	0	0	0
Bacillariophyceae	*Chaetoceros danicus* P.T.Cleve, 1889	80	812	0	15116	478	2703	3083	420	0	3419	1909	160	520	0	20	0	0	0
Bacillariophyceae	*Chaetoceros debilis* P.T. Cleve, 1894	42320	10042	10816	12367	31721	7500	15210	39519	2112	0	0	0	0	2400	20	0	0	220
Bacillariophyceae	*Chaetoceros* cf *debilis* P.T. Cleve, 1894	0	8225	6015	1995	0	0	0	0	0	0	0	0	0	160	0	0	0	0
Bacillariophyceae	*Chaetoceros decipiens* Cleve, 1873	0	2941	0	0	0	68	4802	630	0	0	588	400	0	0	0	0	0	0
Bacillariophyceae	*Chaetoceros diadema* (Ehrenberg) Gran, 1897	0	0	0	14318	273	0	0	0	0	0	0	0	0	0	0	0	0	0
Bacillariophyceae	*Chaetoceros didymus* Ehrenberg, 1845	0	0	0	0	6667	0	0	0	0	0	0	0	0	0	0	0	0	0
Bacillariophyceae	*Chaetoceros eibenii* Grunow in Van Heurck, 1882	720	0	6874	0	0	0	1608	0	0	32238	73170	0	0	0	0	0	0	0

Bacillariophyceae	*Chaetoceros furcellatus* Bailey, 1856	0	1422	0	45067	0	0	0	105	0	0	0	480	0	0	0	0	0	0
Bacillariophyceae	*Chaetoceros laciniosus* Schütt, 1895	0	1929	0	499	0	0	0	105	0	0	0	0	0	0	0	0	0	0
Bacillariophyceae	*Chaetoceros lorenzianus* Grunow, 1863	0	0	8112	0	0	0	0	0	0	13333	0	0	0	0	0	0	0	0
Bacillariophyceae	*Chaetoceros* cf *lorenzianus* Grunow, 1863	0	0	2363	0	273	0	2681	0	0	6350	2056	1360	0	0	0	0	0	0
Bacillariophyceae	*Chaetoceros radicans* F.Schütt, 1895	0	0	32448	4507	0	4473	38830	0	0	31750	0	0	0	0	0	0	0	0
Bacillariophyceae	*Chaetoceros similis* P.T. Cleve, 1896	0	0	0	0	0	0	0	0	0	0	2203	0	0	0	0	0	0	0
Bacillariophyceae	*Chaetoceros socialis* H.S.Lauder, 1864	2522880	786005	744802	1000480	253333	95000	9604	4988889	1995680	1593333	6384640	52480	29167	24560	0	80	27650000	660
Bacillariophyceae	*Chaetoceros* cf *socialis* H.S.Lauder, 1864	0	0	5408	0	0	0	7203	0	0	0	0	400	0	0	1820	200	0	160
Bacillariophyceae	*Chaetoceros tenuissimus* Meunier, 1913	3840	0	0	18027	0	0	0	0	3333	0	5120	0	0	0	0	0	0	0
Bacillariophyceae	*Chaetoceros wighamii* Brightwell, 1856	1920	35802	18928	13520	23675	0	12005	0	0	0	0	0	0	0	0	0	0	0
Bacillariophyceae	*Chaetoceros* cf *wighamii* Brightwell, 1856	0	0	0	0	0	0	2145	0	0	0	441	0	0	0	0	0	0	0
Bacillariophyceae	*Chaetoceros* sp.	56720	111765	57922	29334	67828	20000	161572	92467	13521	65142	277949	2000	79207	1400	2800	40	0	820
Bacillariophyceae	*Climaconeis* cf *delicatula* (Cleve) E.J.Cox, 1982	0	0	0	0	0	0	0	0	0	0	0	0	0	40	0	0	0	20
Bacillariophyceae	*Cylindrotheca closterium* (Ehrenberg) Reimann & J. Lewin, 1964	160	1523	859	0	1434	1288	268	0	0	0	441	80	0	120	40	0	432	20
Bacillariophyceae	*Eucampia groenlandica* Cleve, 1896	0	0	0	0	0	0	268	0	0	3419	0	0	0	0	0	0	0	0
Bacillariophyceae	*Eucampia* sp.	0	0	0	0	0	0	0	0	0	0	0	160	0	0	0	0	0	0
Bacillariophyceae	*Fragilariopsis oceanica* (Cleve) Hasle, 1965	1120	0	0	0	0	0	0	0	0	0	0	0	0	0	0	0	0	0
Bacillariophyceae	*Fragilariopsis* sp.	0	9342	0	6183	6667	9150	2401	0	0	17584	0	0	12500	0	80	0	0	0
Bacillariophyceae	*Guinardia cylindrus* (Cleve) Hasle, 1996	0	0	0	0	68	0	0	0	0	0	0	0	0	0	0	0	0	0
Bacillariophyceae	*Guinardia tubiformis* (G.R.Hasle) Hasle, 1996	80	0	0	0	0	0	0	0	0	0	0	0	0	0	0	0	0	0
Bacillariophyceae	*Leptocylindrus danicus* P.T. Cleve, 1889	1200	4874	1504	5685	24319	2711	1742	315	1643	0	0	160	240	0	0	0	0	0
Bacillariophyceae	*Leptocylindrus minimus* Gran, 1915	640	914	4726	1795	4164	1084	0	0	2347	0	1616	1680	0	0	0	0	0	80
Bacillariophyceae	*Melosira* sp.	0	0	0	0	478	0	0	0	0	0	0	0	0	0	0	0	0	0
Bacillariophyceae	*Navicula* cf *distans* (W.Smith) Brébisson, 1854	80	0	0	0	0	0	0	0	0	0	0	0	0	0	0	0	0	0
Bacillariophyceae	*Navicula* sp.	0	0	0	0	0	0	0	0	0	0	0	0	0	0	0	800	0	0
Bacillariophyceae	*Nitzschia* sp.	0	406	0	0	0	0	134	0	0	0	0	0	0	0	0	0	0	0
Bacillariophyceae	*Odontella aurita* (Lyngbye) C.Agardh, 1832	0	0	0	9013	0	0	0	0	0	0	0	0	0	0	0	0	0	0
Bacillariophyceae	*Phaeoceros* sp.	0	203	10816	0	0	203	0	210	0	0	0	0	0	0	0	0	0	0

Bacillariophyceae	*Phaeodactylum tricornutum* Bohlin, 1898	0	0	0	0	0	339	0	0	0	0	0	0	0	0	60	0	0	0
Bacillariophyceae	*Porosira glacialis* (Grunow) E. Jørgensen, 1905	240	0	0	0	0	0	0	0	3755	0	0	320	0	0	0	0	1728	0
Bacillariophyceae	*Pseudo-nitzschia* cf *pungens* (Grunow ex P.T. Cleve) Hasle, 1993	0	0	0	0	0	0	938	0	0	0	441	0	0	0	0	0	0	0
Bacillariophyceae	*Pseudo-nitzschia seriata* (Cleve) H.Peragallo, 1899	240	406	0	698	0	136	0	0	0	0	0	0	0	0	0	0	0	0
Bacillariophyceae	*Rhizosolenia borealis* B.G.Sundström, 1986	0	0	430	0	0	0	0	0	0	0	0	0	0	0	0	0	0	0
Bacillariophyceae	*Rhizosolenia setigera* Brightwell, 1858	80	305	644	499	273	68	0	0	235	0	0	0	0	0	0	0	0	0
Bacillariophyceae	*Rhizosolenia styliformis* Brightwell, 1858	80	0	0	0	0	0	0	0	0	0	0	0	0	0	0	0	0	0
Bacillariophyceae	*Thalassiosira antarctica Comber*, 1896	0	1015	0	997	0	0	938	630	0	0	1322	0	0	0	0	0	0	0
Bacillariophyceae	*Thalassiosira* cf *eccentrica* (Ehrenberg) P.T. Cleve, 1904	0	508	0	0	0	0	0	1155	0	0	0	0	0	0	0	0	0	0
Bacillariophyceae	*Thalassiosira gravida* P.T. Cleve, 1896	960	102	0	0	0	0	0	0	0	0	0	0	0	0	0	0	0	0
Bacillariophyceae	*Thalassiosira* cf *gravida* P.T. Cleve, 1896	960	0	0	0	0	0	0	0	0	0	0	0	0	0	0	0	0	0
Bacillariophyceae	*Thalassiosira nordenskioeldii* P.T. Cleve, 1873	2800	0	215	0	0	0	6166	0	469	4396	734	0	0	0	0	0	0	0
Bacillariophyceae	*Thalassiosira punctigera* (Castracane) Hasle, 1983	0	203	215	1197	1366	136	0	840	0	0	147	0	0	80	0	0	0	100
Bacillariophyceae	*Thalassiosira* cf *punctigera* (Castracane) Hasle, 1983	480	0	0	0	0	0	0	0	0	0	0	0	0	0	0	0	0	0
Bacillariophyceae	*Thalassiosira* sp.	480	508	430	0	0	610	670	3254	1878	977	294	1600	80	320	380	80	25062	120
Bacillariophyceae	Diatom sp.	0	0	0	0	0	68	0	0	0	0	147	0	0	0	0	0	25432	20
Bacillariophyceae	Pennate diatom sp.	0	0	0	0	0	68	0	0	0	0	0	160	0	0	0	0	0	0
Chlorophyta	Chlorophyceae sp.	38400	0	0	0	0	0	0	0	0	0	0	0	0	0	0	40	0	0
Chlorophyta	Prasinophyceae sp.	3840	2941	2704	18027	0	2500	0	0	0	0	0	0	45833	0	0	0	0	20
Chlorophyta	*Pyramimonas* sp.	0	0	0	0	0	0	0	0	0	0	0	0	0	0	0	0	0	160
Chrysophyceae	Chrysophyceae sp.	0	0	2704	4507	16667	0	9604	0	0	3333	5120	80	0	0	20	200	0	440
Chrysophyceae	Chrysophyceae cf *dinobryon*	0	0	0	13520	0	5000	0	0	3333	3333	5120	80	0	0	0	0	0	80
Chrysophyceae	*Dinobryon balticum* (Schütt) Lemmermann, 1901	57600	61765	5408	117173	46667	20000	314531	94444	0	346667	163840	1040	7320	40	20	40	0	0
Cryptophyceae	Cryptophyceae sp.	7680	2941	0	22533	16667	0	0	0	0	0	0	160	0	200	0	0	0	60
Dictyochophyceae	*Ciliophrys infusionum* Cienkowski, 1876	0	0	0	0	0	0	4802	0	0	0	0	80	0	0	20	0	0	20
Dinoflagellata	*Alexandrium* sp.	0	0	0	0	0	0	0	0	0	0	0	0	0	0	0	0	0	0
Dinoflagellata	*Centrodinium punctatum* (Cleve) F.J.R.Taylor, 1976	0	0	0	0	0	0	0	0	0	0	147	0	0	0	0	0	0	0
Dinoflagellata	*Corythodinium* sp.	0	0	0	0	68	68	0	0	0	0	0	0	0	0	0	0	0	0

Dinoflagellata	*Dinophysis acuminata* Claparède & Lachmann, 1859	80	0	0	0	68	0	0	0	0	0	147	0	0	0	0	0	0	0
Dinoflagellata	*Dinophysis acuta* Ehrenberg, 1839	80	102	0	0	0	0	0	0	0	0	0	0	0	0	0	0	0	0
Dinoflagellata	*Dinophysis* cf *acuta* Ehrenberg, 1839	0	0	0	100	0	0	0	0	0	488	0	0	0	0	0	0	0	0
Dinoflagellata	*Dinophysis* cf *norvegica* Claperède & Lachmann, 1859	0	0	215	0	0	0	0	0	0	0	0	0	0	0	0	0	0	0
Dinoflagellata	*Gymnodinium arcticum* Wulff, 1919	0	0	0	0	0	0	0	105	0	0	0	0	0	0	0	0	0	0
Dinoflagellata	*Gymnodinium gracile* Bergh, 1881	0	0	0	0	0	0	134	0	0	0	0	0	0	0	0	0	0	0
Dinoflagellata	*Gymnodinium* sp.	0	711	0	9911	137	2636	1206	105	0	0	5708	80	0	80	0	440	0	100
Dinoflagellata	cf *Gymnodinium*	0	0	0	499	0	0	0	0	0	0	0	0	0	0	0	0	0	0
Dinoflagellata	*Gyrodinium spirale* (Bergh) Kofoid & Swezy, 1921	0	0	0	0	137	0	0	210	0	488	0	0	80	0	0	0	0	0
Dinoflagellata	*Gyrodinium* sp.	0	0	0	0	137	0	0	0	0	0	294	0	120	0	0	0	0	20
Dinoflagellata	*Kapelodinium* cf *vestifici* (Schütt) Boutrup, Moestrup & Daugbjerg, 2016	0	0	0	0	0	68	0	0	0	0	0	0	0	0	0	0	0	0
Dinoflagellata	*Lebouridinium glaucum* (Lebour) F.Gómez, H.Takayam, D.Moreira & P.López-García, 2016	0	0	0	199	205	0	0	0	0	488	147	0	0	0	0	0	0	20
Dinoflagellata	*Micracanthodinium claytonii* (R.W.Holmes) J.D.Dodge, 1982	0	0	0	0	0	0	0	0	0	0	0	0	0	0	0	0	432	0
Dinoflagellata	*Oxytoxum* cf *scolopax* F.Stein 1883	0	305	0	0	0	0	0	0	0	0	0	0	0	0	0	0	0	140
Dinoflagellata	*Oxytoxum* sp.	0	0	0	598	0	271	938	1050	469	1465	1175	720	0	80	240	280	4321	360
Dinoflagellata	*Peridiniella catenata* (Levander) Balech, 1977	0	1625	0	1197	137	0	0	105	0	6350	1469	0	3160	0	0	520	0	0
Dinoflagellata	*Peridinium* sp.	0	711	0	0	0	271	0	105	0	0	147	80	40	0	0	0	432	60
Dinoflagellata	*Protoperidinium bipes* (Paulsen) Balech, 1974	0	0	0	199	68	203	0	2205	235	488	734	320	200	40	0	0	1296	0
Dinoflagellata	*Protoperidinium brevipes* (Paulsen) Balech, 1974	0	0	0	0	0	68	0	0	0	0	0	0	0	0	0	0	0	0
Dinoflagellata	*Protoperidinium steinii* (E. Jørgensen) Balech, 1974	0	0	0	0	0	0	0	105	0	0	0	0	0	0	0	0	0	0
Dinoflagellata	*Protoperidinium* sp.	0	0	215	0	0	68	134	0	235	0	147	0	0	0	0	0	0	0
Dinoflagellata	*Pyrophacus* sp.	80	0	0	0	0	0	0	0	0	0	0	0	0	0	0	0	0	0
Dinoflagellata	*Tripos longipes* (Bailey) F.Gómez, 2013	0	0	0	199	0	0	134	0	0	0	0	0	0	0	0	0	0	0
Dinoflagellata	Dinoflagellate sp.	5040	711	5926	15016	4426	136	3875	11426	939	2442	881	960	200	360	400	1360	3456	40
Dinoflagellata	Thecate dinoflagellate sp.	0	0	0	798	273	474	402	1155	0	1954	881	0	0	480	0	40	0	380
Euglenophyceae	Euglenophyceae sp.	3840	0	0	4507	0	0	0	0	0	0	0	0	0	40	0	0	0	0

Euglenophyceae	*Trachelomonas* sp.	0	0	0	4507	0	0	0	0	0	0	0	0	0	0	0	0	0	0
Haptophyta	*Phaeocystis* sp.	0	0	0	0	0	1762	0	3989	15256	0	0	0	0	0	0	0	0	0
Xanthophyceae	*Meringosphaera mediterranea* Lohmann, 1903	0	0	0	0	0	0	0	0	0	0	0	0	0	0	0	0	0	20
	Unidentified flagellate	19200	41176	5408	31547	36667	35000	55223	16667	10000	16667	31014	400	291667	600	80	480	25864	1360
	Unidentified cells 2-20 µm	80	12272	2704	45466	16667	37703	12541	22642	0	0	5120	400	16987	560	180	200	432	220
	Unidentified cells 25-80 µm	560	1929	0	798	0	0	268	210	939	488	881	80	1000	0	40	120	0	100
	Cell cf. C. sosiales	15360	0	5408	0	13333	0	0	261111	0	0	0	0	0	0	0	0	0	0
	Cell cf. C. Wighamii	0	0	0	0	0	0	0	0	0	0	0	0	0	2200	0	0	0	0

Appendix 2: Primary productivity per depth in full stations

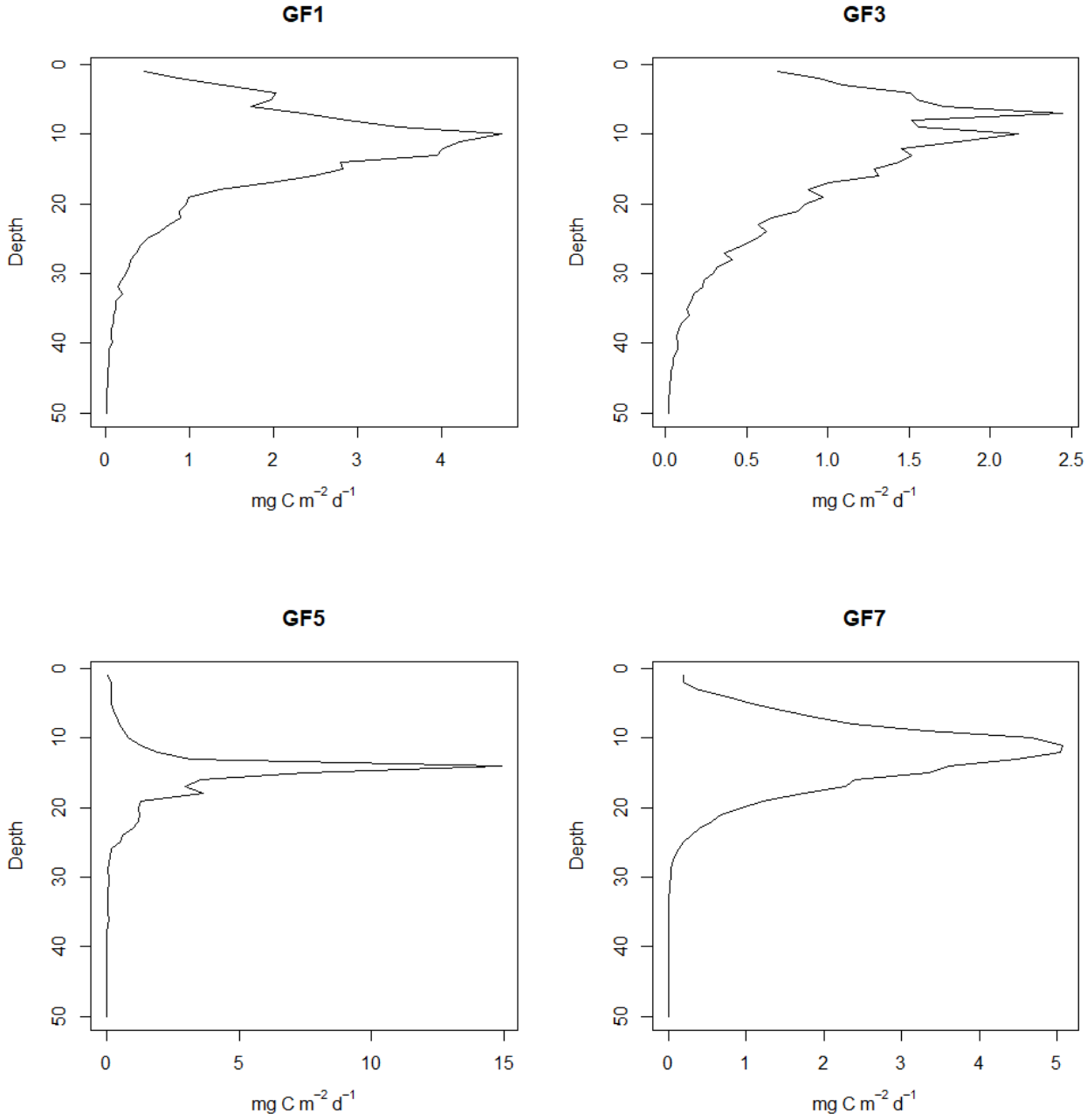

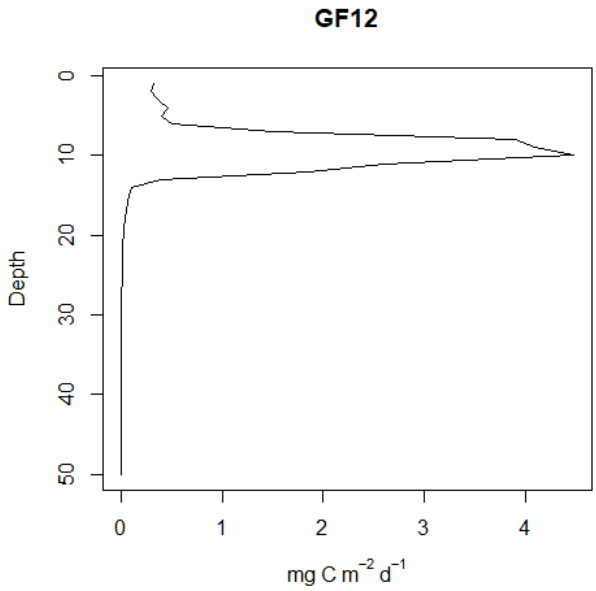
GF12
Depth
0
10
20
30
40
50
0
1
2
3
4
mg C m^{-2} d^{-1}

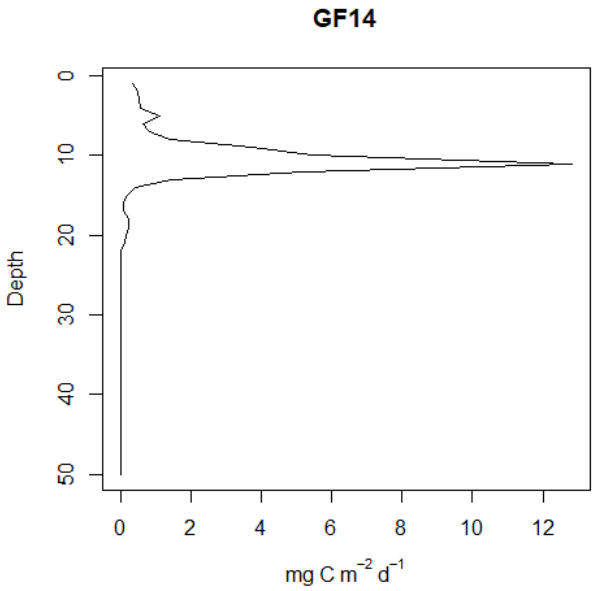
GF14
Depth
0
10
20
30
40
50
0
2
4
6
8
10
12
mg C m^{-2} d^{-1}